

Supplementary Materials for **Strong male bias drives germline mutation in chimpanzees**

Oliver Venn, Isaac Turner, Iain Mathieson, Natasja de Groot, Ronald Bontrop, Gil McVean*

*Corresponding author. E-mail: mcvean@well.ox.ac.uk

Published 13 June 2014, *Science* **344**, 1272 (2014)
DOI: 10.1126/science.344.6189.1272

This PDF file includes:

Materials and Methods
Supplementary Text
Figs. S1 to S12
Tables S1 to S11
References

Strong male bias drives germ line mutation in chimpanzees

Oliver Venn, Isaac Turner, Iain Mathieson, Natasja de Groot, Ronald Bontrop, Gil McVean

Supplementary Information

Contents

1.	Method summary.....	3
2.	Samples.....	3
3.	DNA extraction and sequencing.....	4
4.	Read-mapping, variant calling and filtering	4
	Mapping-based variant calling.....	4
	Assembly-based variant calling.....	4
5.	Intersection call set	5
6.	Inferring recombination events and transmission across the genome	5
7.	Scaffold refinement.....	7
	Chromosome X.....	8
	Pseudoautosomal region (PAR).....	8
	Non-PAR.....	9
8.	Classification of sites inconsistent with the inferred transmission.....	9
9.	Identification and validation of de novo base substitutions	10
	Mask.....	10
	Evidence filter.....	11
	Purity filter.....	11
	Consistency filter.....	11
	Validation against segregating variation in Western Chimpanzees.....	12
	Validation through re-genotyping	12
	Manually curated set	12
10.	De novo mutation clustering.....	13

11.	Impact of sequence features on de novo mutation rates	13
12.	Estimation of de novo mutation false negative rate.....	13
13.	Determining the phase of de novo mutations.....	14
	Direct phasing from read-pair data.....	14
	Phasing through transmission in individual F.....	14
14.	Estimating male-bias (alpha)	14
15.	Estimating mutation rates.....	15
	Estimating female- and male-specific mutation rates without parent-of-origin information.....	15
	Estimating female- and male-specific contributions using parent-of-origin information	16
	Per year estimates of the mutation rate	16
16.	Estimates of human-chimpanzee divergence from genome alignments	16
17.	Supplementary figure legends.....	18

1. Method summary

The genomes of a nine-member three-generation Western Chimpanzee pedigree were sequenced (100 bp paired-end reads with 450 bp average insert) from whole blood using Illumina HiSeq instruments (Illumina, CA) and mapped to the panTro3 reference (26). SNVs and small indels were called and filtered without incorporating pedigree information through both mapping- (27, 28) and assembly-based (14) methods. Transmission vectors were inferred from the intersection of the call sets through a two-step process. First, a robust version of the Lander-Green algorithm was applied over 1Mb intervals, using the proportion of sites concordant with each transmission vector rather than likelihoods. Only single crossover events between intervals were permitted. Second, cross-over breakpoints were refined locally, using posterior decoding of the standard algorithm, incorporating uncertainty on the inferred genotype through genotype likelihoods. We defined breakpoints from the 95 percent credible interval for single event compatible transitions. Among all sites called by the mapping approach we identified positions where the reported genotypes were inconsistent with the inferred transmission vector. For such sites, we compared the likelihood of different models conditional on the transmission vector: segregating variant, de novo mutation, single gene conversion, segregating deletion, erroneous call. Candidates were then filtered on evidence (log-likelihood of de novo mutation model > 5 units higher than any other model), purity (no evidence for the variant allele in any other sample apart from offspring), and consistency (candidates segregate according to the inferred local transmission). The false positive rate was assessed through genotyping a subset of de novo mutations through a primer-extension assay (Sequenom, CA), and the false negative rate through allele-dropping simulations. The impact of paternal age on de novo mutation was calculated through Bayesian linear regression allowing for individual-specific false negative rates.

2. Samples

Nine individuals from a 3-generation Western chimpanzee (*Pan troglodytes verus*) pedigree were housed in a colony at the Biomedical Primate Research Centre (Rijswijk, Netherlands). Individuals C-I were born at the Centre; individuals A and B were caught from the wild. No disorders or syndromes are reported for the individuals. We verified reported genders by calculating the total heterozygous genotype call frequency on the X chromosome for male and female samples (P-value 0.007, unpaired t-test on observed X chromosome heterozygosity between genders). We also evaluated relatedness between individuals by calculating the Pearson correlation between individuals' genotype vectors excluding monomorphic sites and sites with missing genotypes. The observed pairwise correlation between individuals is concordant with their expected relatedness (Figure S2). Dates of birth were obtained from Centre records (estimates for A and B), and age at conception estimated using a gestation estimate of 0.621 years (29).

3. DNA extraction and sequencing

Blood samples were supplied under the EUPRIM-Net EU contract RII-026155 and CITES approval. DNA was extracted from peripheral blood mononuclear cells using affinity bead selection (Qiagen, Netherlands), and 100 bp paired-end shotgun libraries, with an average insert of 450 bp, were constructed. Libraries were sequenced on Illumina HiSeq 2000 instruments using standard chemistry and vendor provided base calling software, generating 0.9 Tb of sequence (Table S1).

4. Read-mapping, variant calling and filtering

Reads were aligned to the CGSC 2.1.3/panTro3 chimpanzee reference genome using Stampy (27) resulting in an average mapped coverage of 35x, and 90.8% of the aligned genome covered by at least 15 reads (Table S1).

Mapping-based variant calling

Variants were called using Platypus (version 0.2.1; www.well.ox.ac.uk/platypus) with default settings, treating samples as coming from unrelated individuals (family relationships used in downstream analyses). No adjustments were made for chromosome X. Variants were then filtered based on sequence context, with only variants satisfying all the following criteria retained:

- Variant does not lie in a homopolymer (run of the same base) of length 6 or more.
- Variant does not lie in a tandem repeat of length 10 or more.
- Not all samples are homozygous for the alternative allele.
- Fewer than 5 other variants are within +/- 25bp window.
- Variant has a single alternative allele.
- Variant does not lie in a predicted indel hotspot (30).

After filtering, we retained 3,957,360 single nucleotide variants (SNVs). Of these sites, 2,853,842 (66%) had been detected in an earlier study with partially overlapping samples (18). The overall transition/transversion ratio was 2.24 (2.28 and 2.18 for sites which had, or had not, been detected in (18)). We also called 169,387 small indels.

Assembly-based variant calling

Variants were called with the de novo assembler and variant caller Cortex (14). De Bruijn graphs were built for each sample with k=31, and in doing so PCR duplicates were removed. Reads were also broken at homopolymer runs longer than 8bp and at bases with base quality less than 5. Graphs were individually cleaned of low frequency contigs to remove sequencing error. Calling was performed with the 'Joint' pipeline (31). The reference genome was not used in calling. For the population filter, putative variants sites were filtered out if the relative likelihood of the variant

model was less than 10 times greater than repeat or error models. Variants whose 5' flank did not map with MAPQ ≥ 30 were discarded. Cortex called 3,400,416 bubbles, resulting in 3,727,902 variants of which 2,981,175 (80%) variants passed the filters.

5. Intersection call set

To identify a high quality subset, we intersected the mapping- and assembly-based calls (henceforth referred to as the intersection call set) leaving 1,595,502 sites with an overall transition/transversion ratio of 2.24. The genotypes (and genotype likelihoods) inferred through the mapping approach were assigned to the intersection call set.

6. Inferring recombination events and transmission across the genome

To reconstruct the patterns of descent of the parental chromosomes, we implemented a robust Lander-Green algorithm (32) to jointly infer the phase of parental genotypes and their transmission to children (the transmission vector). The standard Lander-Green approach is sensitive to mis-specified genotypes and false-positive errors (33), which cause artifactual switches between states. To guard against such errors, we used a two-stage approach. First, we inferred a transmission vector scaffold across non-overlapping intervals using a robust approach and allowing for at most one recombination event between intervals and none within. Informed by LD-based estimates of recombination in chimpanzees (18), we chose an interval size of 1 Mb, so that we would expect at most one recombination event per interval. Second, we fine-mapped the location of inferred crossovers. Details of the inference method are given below.

The Lander-Green algorithm is a hidden Markov model (HMM) in which the hidden states are transmission vectors and emissions are the genotypes at each locus. Transmission vectors are binary vectors of length two times the number of children that describe which grandparental chromosome (grandpaternal or grandmaternal) is inherited for each child. Let the number of genotyped children be n . For each child i in $\{1, 2, \dots, n\}$, let $V^{i,m}$ and $V^{i,p}$ be the maternal and paternal transmission indicators respectively, where $V^{i,m}(s)$ is 0 if the grand-maternal chromosome is inherited and 1 if the grand-paternal chromosome is inherited from the mother at site s , and similarly defined for the father. There are 2^{2n} possible transmission vectors.

To infer the transmission vector scaffold, we calculate the number of sites compatible with each potential underlying transmission vector. Let l represent the range of a chromosome interval and S the set of variant sites in l . We then calculate, C_j^l , the Mendel consistent proportion, defined as the

fraction of sites compatible with transmission vector V_j , by counting the potential emitted genotypes under V_j that match the genotype that maximises the genotype likelihood $g^*(s)$ at that site

$$C_j! = \frac{1}{|S|} \sum_{s \in S} \delta(g^*(s) \in G(V_j)),$$

where $G(V_j)$ is the set of genotypes induced by projecting the set of all possible phased founder genotype combinations onto V_j and $\delta()$ is an indicator function taking the value 1 if $g^*(s)$ is within the set of possible genotypes and 0 otherwise.

To infer the underlying pattern of transmission across intervals, we implemented a finite state machine (FSM) that takes $\{C_j\}$ as the observation distribution. Transitions in the hidden states of a child represent a change in the chromosome inherited from a parent and thus represent a cross-over event. There are $2n$ possible transitions arising from a single cross-over event. Transitions in the mother and father are independent of each other and independent of the children's hidden states. We assume the probability of more than one cross-over between regions is small since coincident events are expected to be rare between the six children. Conceptually, a cross-over is equivalent to switching the chromosome inherited by a child, hence the size of the set of transmission vectors reached through one cross-over is equal to the number of transmitted chromosomes. To generate cross-over outcomes we specify a function $\rho(V_j(l))$ that generates all potential single cross-over events applied to transmission vector V_j at chromosome interval l .

Costs on transitions in the FSM were imposed to limit switches:

$$(1) \quad p(i \rightarrow j) = 0 \quad \text{if } V_i(l) = V_j(l+1),$$

$$(2) \quad p(i \rightarrow j) = -0.25 \quad \text{if } V_i(l) \in \rho(V_j(l+1)),$$

$$(3) \quad p(i \rightarrow j) = -\infty \quad \text{otherwise.}$$

Case 1 represents no cross-over, Case 2 represents a single cross-over in a child, and Case 3 represents multiple cross-overs in the same interval, which are ignored. Note costs are in log units.

The transition costs were chosen heuristically, but we note that switches were largely insensitive to different penalty values. We used the Viterbi algorithm to identify the highest scoring transmission vector sequence across intervals for each chromosome.

7. Scaffold refinement

To improve the resolution of the cross-overs inferred across chromosome intervals, we implemented a modified HMM to use all available SNVs and analyzed each event separately (others have used similar constrained fine-mapping approaches (34)). We used the Forward-Backward algorithm applied to SNVs in the 1Mb surrounding cross-over regions identified at the transmission vector scaffold level.

To incorporate genotype uncertainty we computed transmission likelihoods from genotype likelihoods. Each family structure defines the set of transmission vectors \mathcal{V} compatible with Mendelian transmission and consequently induces the set of potential genotypes \mathcal{G} . At a site, we compute the likelihood of a transmission vector V_j where j in $\{1, 2, \dots, 2^{2n}\}$ at site s as,

$$L(V_j|s) \propto P(s|V_j) = \sum_{g \in G(V_j)} P(s|g)P(g),$$

where $G(V_j)$ is the set of genotypes induced by projecting the set of all phased founder genotype combinations on V_j , and $P(s|g)$ is the genotype likelihood at site s for genotype g . We use a uniform prior for $P(g)$; i.e. each genotype vector that is compatible with the transmission vector is assumed to be equally likely. Because the data are typically strong, our inferences are only weakly affected by the choice of the prior.

Since each transmission vector induces a set of potential genotype vectors given the founder genotypes, we can use linear algebra and pre-calculated tables of the mapping between \mathcal{G} and \mathcal{V} to rapidly index the genotype likelihoods in the likelihood calculation.

We represent the full state matrix of transmission as,

$$(1) \quad p(i \rightarrow j) = 1 - 12/A \quad \text{if } V_i(s) = V_j(s+1),$$

$$(2) \quad p(i \rightarrow j) = 1/A \quad \text{if } V_i(s) \in \rho(V_j(s+1)),$$

$$(3) \quad p(i \rightarrow j) = 0 \quad \text{otherwise.}$$

The probability of a switch, $1/A$, was assessed empirically and a value of $A = 1000$ was selected. We incorporated the scaffold information by constraining the initiating and terminating states to be those inferred from the window-based analysis (see previous section). We then used posterior decoding to determine the location of the candidate cross-over event, assessed as the switch in posterior probability dominance for the two states. Cross-over breakpoints were defined to be the 95% credible interval between transmission vector change points between the scaffold-determined

initiating and terminating states. The credible interval was calculated as the interval containing a 95% change in the posterior decoding for the initiating and terminating states requiring symmetry in the change for both states and consistency within the interval. If the decoding failed these checks the region was flagged as ‘complex’ and was set to the transmission for the initiating state. Of the 375 cross-over events identified, 6 were defined to be ‘complex’ showing evidence for a double cross-over nearby to a single cross-over event (Table S2). Including the complex events, the median credible interval was 8,752 bp, spanning 5 variant sites (Table S3).

To visualize information about cross-over breakpoint resolution, we plotted the relative likelihoods of the five best ranking transmission vectors versus the inferred transmission vector after refinement (Figure S3). The majority of sites are well resolved, though there are both artifacts (e.g. chromosome 9 mis-assembly at c. 155 Mb) and possible missed events (e.g. potential double cross-over on chromosome 1 at 200 c. Mb). We also took the 192 cross-over intervals from the intersection set localization resolved to less than 10 kb and plotted the average LD-based recombination rates in Western chimpanzees (*18*) around their midpoints. Reassuringly we see strong (c. 3.7-fold) increase in LD-based recombination rates at these locations (Figure S6), serving to validate both datasets.

The total genetic map length was calculated by applying the Kosambi map function (*35*) for 12 meioses to the total number of detected crossovers.

Chromosome X

To analyse the X chromosome, we separated the pseudoautosomal region (PAR) from the rest of chromosome. Since the location of the PAR has not been defined in the chimpanzee reference genome, we defined the PAR as the human reference (GRCh37) PAR1 coordinates mapped to panTro3 coordinates (by mapping the GRCh37 PAR interval to panTro3 coordinates through syntenic alignments using the UCSC liftOver tool (*36*) this operation is known as liftOver). The panTro3 PAR coordinates were chrX:43,989-2,693,334. We analysed the PAR as for autosomes (described above) and modified the set of transmission vectors and the induced genotype vectors accordingly for the non-PAR to allow for hemizygous states in males. We retained apparent heterozygous sites on the male X.

Pseudoautosomal region (PAR)

The high repeat content of the PAR makes its assembly difficult. In the chimpanzee reference the PAR is covered by 214 contigs with a median length of 1,734 bp. There are almost no contigs between 0.8 Mb and 1.4 Mb. Nevertheless there are five contigs with length greater than 20 kb mapped to each end of the PAR. Inspection of alignments at these contigs indicated good mapping.

Given the contig spacing, we expect to have power to detect events separated by at least 0.13 Mb but may miss events occurring over shorter distances (Table S4). Since cross-overs are rare events, we therefore decided to infer the transmission patterns across the PAR using the five largest contigs.

Across the 5 contigs we detect 5 cross-overs; 4 paternal events in E, G, and two in I, and 1 maternal event in G (Table S4). To check for consistency, we also inferred transmission vectors over 1 Mb intervals, as was done for the autosomes. We recovered events in D and E, the only events detectable at a 1 Mb scale. We also inferred a cross-over in the grand-paternal chromosome transmitted to F which could indicate a double cross-over arising in the interval between the second and third 20 kb contigs, however this is also difficult to distinguish from a signal arising from mis-assembly. We therefore, do not include this event(s) in computing Table S5.

Non-PAR

To analyse the non-PAR region of chromosome X, we generated a set of X-specific emission and transmission probabilities. Through this approach we detected 9 female-specific cross-over events in the children: 3 in D, 1 in E, 1 in F, 1 in G, 1 in H, and 2 in I.

8. Classification of sites inconsistent with the inferred transmission

To distinguish between instances of segregating variant, *de novo* mutation, segregating deletion, gene conversion, and error, we calculate the likelihood of each model conditional on the transmission vector scaffold and the data observed at sites where the genotypes were inconsistent with the inferred transmission vector. We incorporate genotype uncertainty using the reported genotype likelihoods obtained from the mapping-based variant calling.

Here we define each of the five models. It is intuitive to think of the generative model for each scenario to inform the likelihood calculation under each model. We generate the potential genotypes conditional on the transmission vector scaffold at that site; this can be made efficient through pre-calculating lookup tables to index genotype likelihood values.

Segregating variant. We model a segregating variant as those genotypes compatible with the inferred transmission vector V_j , i.e. $\{G(V_j)\}$. Under this model, genotypes incompatible with the transmission vector only *arising* from genotyping error.

De novo mutation. We model non-recurrent mutations arising at sites where the founders are homozygous. To generate the potential genotypes under this mutation model we introduce mutations to each of the transmitted founder chromosomes and then allow the alleles to descend through the pedigree according to the inferred transmission. Although recurrent mutations do arise,

mutations of this form are rare and hard to distinguish from mis-alignments and are therefore not modelled. We also chose not to model mutations that arise on heterozygous backgrounds because such events are difficult to distinguish from mis-alignment and mis-calibrated genotype calls.

Segregating deletion. Segregating deletions result in unexpected homozygosity in the children. To model this effect, as with de novo mutations, we consider possible deletion genotypes in the founders and use the inferred transmission vector to define the set of possible genotypes in the children. To guard against assembly-driven false positives we require that least one founder has a reference compatible haplotype.

Gene conversion. We model single site gene conversions as site-specific changes in the chromosome inherited by one of the children allowing only one cross-over, i.e. requiring that a switch to a new transmission vector V_i satisfies $V_i \in \rho(V_{j,\text{scaffold}})$. Here, genotypes show no Mendel error, but are inconsistent with the inferred transmission vector.

Error. We model errors by identifying the maximum likelihood vector genotype irrespective of any constraint.

9. Identification and validation of de novo base substitutions

To guard against false positives arising through differential mapping between individuals, we constructed a genome mask across the alignments, we then identified de novo point mutation candidates in the alignment-based calls using filters on evidence, purity and consistency.

Mask

To avoid potential contamination from regions with sparse coverage that may induce false negatives and mis-assembled regions and/or mis-alignments, we generated a genome mask across individuals. First we applied the GATK CallableLoci module (37) to each sample's alignment using the following parameters:

- The fraction of reads with mapping quality ≤ 1 exceeds 0.1
- The number of aligned reads < 4 , where reads must have a mapping quality ≥ 10 and base quality ≥ 20 to be counted

We then identified regions of the genome that passed filters in all individuals generating a single mask. Of the 3,307,943,878 bases in panTro3, we identified 2,537,740,297 bases (91.2% of the mappable reference genome, i.e. excluding bases called as N and gaps) across the individuals that satisfied the criteria (Table S9).

Next to incorporate the impact of the reference-based filters applied to the alignment-based calls, specifically the homopolymer, tandem repeat, and indel hotspot filters (see Mapping-based variant calling Section), we identified all regions in the reference sequence that would fail these filters and subtracted them from the mask resulting in 2,472,016,029 bases (89.8% of the mappable reference genome, Table S9).

Within the mask there were 25,212 sites with Mendel inconsistent genotypes on the autosomes, i.e. de novo mutation candidates. To distinguish de novo mutations from artefacts we applied three filters:

Evidence filter

To identify candidates relative to alternate models, we calculated the relative likelihood between the de novo point mutation model and the next best model. There was a lack of evidence for de novo mutation at the overwhelming majority of Mendel inconsistent sites; only 649 sites across the autosomes had relative log likelihood greater than zero for the de novo point mutation model. For sites with evidence, c. 25 % had a relative likelihood less than 5 (Figure S7). The threshold value was chosen by an iterative threshold-then-check procedure on the Mendel inconsistent calls. First, we identified a high-confidence subset from the candidates as a proxy to assess specificity under the threshold value. Second, we incremented the threshold value, filtered, and then subsampled the highest-ranking candidates that failed filters and manually inspected their alignments to confirm that they were indeed true negatives by checking for transmission consistency, read mapping, and purity. After converging to a threshold value between 4 and 5, we assessed a larger subsample of the candidates now also identifying false-positive candidates. Through this process we chose, a threshold value of 5, which removed all but 337 candidate sites.

Purity filter

To guard against potential false-positives arising through mis-genotyping, we required there be no trace of the mutant allele in any of the reads in founders or children where the variant allele was not called. We obtained counts of reads containing the mutant allele through the Platypus NV field. Note that some reads with reads containing a variant can be missed through this approach because Platypus applies upfront filtering to the reads before NV is calculated.

Consistency filter

Further, we required that all candidates segregate according to the inferred local transmission.

Application of these filters left 204 candidate de novo mutation sites across the autosomes (Table S6, Figure S8) and 3 on the X chromosome. No sites passed the de novo filters in the PAR (Table S6).

Validation against segregating variation in Western Chimpanzees

Previously, we sequenced 10 unrelated chimpanzees (18). Since mutations are rare events, de novo mutation candidates that are also detected as variation segregating in the unrelated individuals are likely to have arisen through false positive errors. To maximize the opportunity to detect errors, we mapped the raw, unfiltered variants called in the 10 chimpanzees (6,869,589 autosomal sites) to panTro3 (6,792,077 sites successfully mapped). None of the 207 candidates were called as variants in the data set.

Validation through re-genotyping

To estimate the false positive rate of the detected de novo mutation candidates, we attempted to validate 93 candidate de novo mutations using the Sequenom platform. The sites were composed of all the detected candidates in individuals E (45 sites) and F (35 sites), and 13 suspected false negatives across all individuals, which were the candidate de novo mutation sites that failed the purity filter, but had only one underlying conflicting read with a low assigned base quality.

Amplicons were designed using Sequenom Typer4.0 software (Sequenom, CA). One site failed amplicon design.

To guard against Sequenom errors arising from (a) PCR amplification based error and (b) measurement error, we duplicated each (a) amplification reactions and (b) assay spotting. Hence each site was genotyped four times in each individual.

Of 92 amplicons, 18 either failed, had inconsistencies across replicates, or mis-calling of the cluster plots. For the remaining sites, we calculated false positive rates under two scenarios. First, we considered a liberal case, where we only required genotype consistency within the trio relevant to the affected individual. Second, we required that the genotypes were consistent across the entire pedigree.

The false positive rate for the remaining sites (having sufficient information) was c. 1.67% (Table S7). Of the 15 potential false negative candidates included in the genotyping panel, 13 were true de novo mutations and 2 were not.

Manually curated set

Inevitably the set of de novo mutation candidates contain some small number of false positives, and a manually curated, conservative call set may be desired - though this comes with the undesirable addition of heuristic filtering strategies. To manually curate the calls, we individually assessed the properties of local alignments around each candidate. If we suspected potential mis-calling, or mis-alignment we marked these sites, this information is recorded in the *is.suspicious* indicator variable in

Table S6, there are 9 such sites. Excluding these sites has a minimal effect on estimates of male bias or the paternal age effect.

10. De novo mutation clustering

To assess the extent of within-sample clustering of de novo mutation events we calculated the number of de novo mutations that lie within a series of distance intervals from other de novo events. We then permuted the location of mutations, thus preserving the total number received by each individual. The permutation was run for 1000 iterations to give the null distribution and the expected counts of co-localised mutations shown in Fig. S9A. Moreover, the simulations were used to calculate a p-value for excess within-sample clustering over a scale of 1Mb. In no simulation was the extent of within-sample clustering as great as that observed).

To ensure that clustering is not the result of regions with poor reference genome quality we repeated the analysis using only the manually-curated variant set (Fig. S9B). This reduced the number of very-closely co-located mutations, but a strong excess of within-sample clustering is still observed ($p < 0.001$).

11. Impact of sequence features on de novo mutation rates

To assess the impact of sequence context, potentially reflecting different mutational processes, on de novo mutation we considered repeat (rmsk), genic (refGene) and assembly-gap tracks downloaded from the UCSC Genome Browser (36).

First we looked for enrichment with proximity to each of the three features assessing significance through permutation. Specifically, we preserved the spacing between events on each chromosome by shifting all bases by a uniformly sampled perturbation distance modulo chromosome length. We found no deviation from the null expectation for each of the three tracks (Figure S10a, b, and c). Furthermore, we observe that point mutation rates show no significant distinction between repetitive and non-repetitive contexts with similar values of alpha and paternal-age effect (Figure S11).

12. Estimation of de novo mutation false negative rate

To estimate individual-specific false negative rates, we used allele-dropping simulations, using empirical distributions of coverage and allele-balance. For each simulated event, we introduced a mutation to the aligned genome at a uniformly sampled location and a founder chromosome, requiring that transmission respect the inferred local transmission. For the affected individual(s) we then allocated the aligned reads drawing from the empirical allele balance distribution, which was

generated from a sample of one million heterozygous sites. We then calculated genotype likelihoods across all the individuals at that site and recorded the true underlying mutation. The false negative rate was then calculated through applying our de novo mutation detection pipeline to the simulated mutations.

Though no transmission vector was enriched for false negatives, we did observe differential false negative rates across the pedigree (Table S8) arising from lower coverage in individual C that resulted in greater genotype uncertainty.

13. Determining the phase of de novo mutations

We used both direct phasing from read-pair data and phasing through transmission in F to assign paternal or maternal origin to de novo point mutations.

Direct phasing from read-pair data

To utilize information in reads and their mate pairs to phase variants in the filtered mapping-based calls, we first filtered low quality reads requiring bases at variant sites have quality > 20 and mapping quality > 30 , then for each individual we assigned haplotypes and calculated strand bias based on the supporting reads.

To phase each de novo mutation, we extracted neighbouring heterozygous sites and used transmission to identify phase and assign maternal or paternal origin.

We assigned parental origin to 61 paternal and 11 maternal mutations through this approach (c. 25% of the candidates).

Phasing through transmission in individual F

We further phased mutations inherited by individual F through transmission to her offspring, assigning 30 events of paternal origin and 5 events of maternal. We note that there was exact agreement between phasing results through transmission and direct phasing for events detected in F.

14. Estimating male-bias (alpha)

We define α as the ratio of the total number of paternal to maternal germ line point mutations. To measure uncertainty in the estimate we use a Bayesian MCMC approach, modelling the observed total counts as independent Poisson-distributed random variables each with an independent uniform (0,1000) prior. We estimate 95% credible intervals from the posterior 95% Equal-Tailed Probability Interval (ETPI).

Using the 11 maternal and 65 paternal phased candidates we estimate $\alpha = 5.26$ (ETPI = 2.93 – 10.47). As a consistency check we also estimate α for individual F because the phase of mutations in this individual was confirmed through two independent approaches. For F we estimate $\alpha = 5.37$ (ETPI = 2.39 – 14.58). If we include the confirmed false negatives from the re-genotyping experiment this increases to 6.21 (ETPI = 2.78 – 16.62).

15. Estimating mutation rates

To estimate the de novo point mutation rate we used Bayesian linear regression to estimate the slope and intercept coefficients for maternal and paternal age effects using all 204 autosomal mutations. To convert to estimates of rates of neutral diversity and divergence we used published estimates of female- and male-specific generation times in the wild (20) and our estimate of the length of accessible genome across the autosomes. We estimated paternal-age effects both with and without using information on the parent of origin.

Estimating female- and male-specific mutation rates without parent-of-origin information

Initial linear model analysis indicated that there is no significant maternal age effect ($P > 0.05$). To provide estimates of coefficients and measure uncertainty in these estimates we used Bayesian linear regression, allowing for a paternal effect only and accounting for variation in false negative rate across the children.

Specifically we analysed d_j , the total number of germ-line point mutations per child j , and the father's age at conception, t_j , to estimate the posterior mean and 95% credible interval for the posterior Equal-Tailed Probability Interval (ETPI) of intercept b_o and slope b_1 . We modelled the number of point mutations as:

$$d_j \sim \text{Pois}(\lambda_j),$$

$$\lambda_j = (b_o + b_1 t_j) \beta_j,$$

where $j \in \{D, E, F, G, H, I\}$ and β_j is the power estimated for child j through the allele-dropping simulations. Priors for coefficients b_o and b_1 specified as uniform(-100, 100), and the likelihood calculated as a Poisson probability.

We then estimated coefficients through rejection sampling, using updates

$$b_o^{i+1} = b_o^i + N(0, \sigma_0^2)$$

$$b_1^{i+1} = b_1^i + N(0, \sigma_1^2).$$

We found that setting σ_0^2 to 2 and σ_1^2 to 0.5 gave a good balance between efficient mixing and convergence. The MCMC was run for 10^6 iterations sampling every 100 iterations and discarding the first 3000 samples.

Estimating female- and male-specific contributions using parent-of-origin information

To use parent of origin information, accounting for variation in power to detect de novo mutations across the pedigree and variable recovery of parent-of-origin information (through read-based and transmission-based phasing), we elaborated the Bayesian linear model above.

We modelled the number of point mutations detected in child j by allowing for separate male- and female-specific intercept terms.

$$d_j \sim \text{Pois}(\lambda_j),$$

$$\lambda_j = (b_{o,f} + b_{o,m} + b_{1,m}t_j)\beta_j, \text{ and}$$

$$n_{j,f} \sim \text{Binom}\left(n_{j,f} + n_{j,m}, \frac{b_{o,f}}{b_{o,f} + b_{o,m} + b_{1,m}t_j}\right).$$

Here, $n_{j,f}$ is the number of de novo mutations in child j of maternal origin and $n_{j,m}$ is the number of paternal origin. Priors for all coefficients were uniform(-100,100), and the likelihood was calculated as the product of a Poisson probability for the parental effect and Binomial probability for the male bias. We used an MCMC approach with rejection sampling to estimate coefficients, again using the Normal distribution as the proposal distribution. The algorithm was run for 10^6 iterations sampling every 100 iterations and discarding the first 3000 samples.

Per year estimates of the mutation rate

To estimate the per year mutation rate we accounted for the proportion of the genome accessible to sequencing and estimated paternal and maternal generation times as the weighted mean of reported values for Western chimpanzees from (20); 26.3 years for females and 24.3 years for males. We then calculated the total number of mutations using the estimated female- and male-specific coefficients for the autosomes, and accounted for effective population size differences on chromosome X by assuming equal population sizes of males and females (i.e. the X chromosome has an effective population size $\frac{1}{4}$ of that of the autosomes). Human parameters were estimated from (7).

16. Estimates of human-chimpanzee divergence from genome alignments

To identify point substitutions between human and chimpanzee lineages, we downloaded the Ensembl EPO 6 primate alignment (release 75) and constructed GRCh37 aligned per chromosome

sequences for human, chimpanzee and orang-utan. We removed EPO alignments where the alignment segment mapped to multiple locations within the same species; we also recorded the locations of indels on the human lineage but removed these events to preserve GRCh37 coordinates. From these aligned sequences we identified substitutions between humans and chimpanzees.

We applied two filters to guard against false-positive substitutions arising from mis-assembly or mis-alignment. First, we filtered out substitutions within 10 bases of an indel or base assigned as N (unknown type). Second, we identified substitutions with more than 5 substitutions within the 12 flanking bases (>5 substitutions in 25 bases) and masked that window.

For the filtered regions we recorded a) the locations of N-bases, and b) the locations of insertions relative to the human lineage in the aligned-chimpanzee sequence, c) the 25 base windows with more than 5 clustered mutations, to generate a divergence mask for the species alignments.

To enable comparison with the observed spontaneous point mutation rate, we identified the regions accessible to both the pedigree sequencing and the species alignments in GRCh37 coordinates (combined mask). We then mapped the de novo mutation candidates (1 autosomal mutation failed liftOver, and 3 X chromosome mutations failed liftOver) and Mendel inconsistent sites from panTro3 coordinates to panTro4 coordinates using the liftOver tool. We applied the combined mask to the substitution candidates and the de novo mutation candidates.

Of the 33,287,505 substitution candidates identified on the autosomes, filter a) removed 65,781, b) removed 2,748,774, and c) removed 422,447 candidates. Furthermore 3,451,952 candidates were removed by applying the combined mask and 542 candidates were removed that overlapped Mendel inconsistent SNVs in the pedigree. We used the remaining 26,598,009 substitutions and 2,204,160,410 bases of unmasked sequence in divergence analyses.

For the X chromosome, we identified 1,295,698 substitution candidates. Filter a) removed 11,915, b) 122,360 and c) 29,236 candidates. The combined mask removed 316,879 candidates and 471 candidates overlapped Mendel inconsistent SNVs. We used the remaining 814,837 substitutions and 86,111,635 bases of unmasked sequence in divergence analyses.

Applying the combined mask to the de novo mutation candidates across the autosomes removed 12 candidates, we re-estimated paternal and maternal effects, values of alpha, and clustering of mutations using the remaining 192 mutation candidates.

To calculate an estimated time to most recent common ancestor (T) between humans and chimpanzees, we estimated mutation rates (μ , bp⁻¹ year⁻¹) and divergence rates (k bp⁻¹) after applying the combined mask. The average number of mutations was calculated using the estimated average paternal and maternal ages for Western chimpanzees (20), accounting for differences in

effective population sizes between males and females on the X chromosome, and substituting in the estimated coefficients for males and females. We then calculated the divergence time as

$$T_i = \frac{k_i}{2\mu_i} \quad \text{where } i \in \{\text{autosome, chromosome X}\}.$$

17. Supplementary figure legends

Figure S1: Data analysis schematic. **A** One hundred base pair paired-end whole genome sequencing data (coloured rectangles) generated from blood samples taken from 9 member Western chimpanzee pedigree (individuals A – I). Hexagons: called variants (~~represented by hexagons~~) identified through assembly (Cortex: variants called independently; orange), and mapping (Platypus after mapping reads to panTro3 using Stampy: variants called and genotyped independently; purple). The intersection call set is identified between mapping- and alignment-based call sets. **B** The partitions of the reference genome where variation can be confidently called are identified across alignments, referred to as the accessible genome. **C** The transmission pattern across chromosomes is inferred from the intersection call set through a two-stage process. First, the transmission pattern is inferred between non-overlapping 1 Mb intervals through a robust implementation of the Lander-Green algorithm. Second, cross-over breakpoints are refined using posterior decoding on a constrained-state HMM using all available sites; grandparental chromosomes differentiated by opacity. **D** The probabilistic classification of sites inconsistent with the inferred transmission. Conditional on the inferred transmission, the likelihood of variation with error, gene conversion, de novo mutation and segregating deletion are calculated. The identified de novo mutation candidates are then filtered for false positive error modes. **E** The remaining candidates are validated through an independent technology to estimate the false positive rate. **F** The power to detect de novo mutations is calculated through simulation on the aligned genomes for each child. **G** Mutation rates, male bias and paternal age are calculated correcting for the estimated power to detect events and the length of the accessible genome.

Figure S2: Relatedness between pedigree individuals. The matrix of values represents the Pearson correlation between two individuals' genotype vectors at intersection sites across the autosomes; cells are coloured by their expected values indicated in the figure legend.

Figure S3: Relative likelihoods for the transmission scaffold. The relative likelihood between the inferred transmission vector (transmission scaffold) and the other five most likely transmission vectors at variant sites in the intersection call set; colours distinguish the relative likelihoods under each transmission vector (compared to the fitted vector). Dotted lines represent the midpoint of the inferred cross-over breakpoints. Values above the x-axis indicate sites for which one of the five alternative transmission vectors is more likely than the scaffold transmission vector. Points above

the $y=0$ axis indicate potential gene conversion events or various error types. Clustered regions (e.g. on chromosomes 2A, 9, 15 and 18) may indicate short cross-over events that have been missed or regions with extensive errors (e.g. arising through structural variation).

Figure S4: The distribution of cross-over events across the autosomes. For each chromosome, represented as grey rectangles, cross-over breakpoints are indicated by lollipops (female, below x-axis) and shovels (male, above x-axis) and the location of centromeres as brown rectangles. Each recipient child is assigned a different colour and distance from the x-axis (see legend). Barplots on the left hand side represent the total number of cross-overs in each individual stratified by grandparental origin.

Figure S5: The relationship between cross-overs and proximity to chromosome telomeres.

A Represented are the mean recombination rate in humans (blue line) from (7) and Western chimpanzees (red line), excluding chromosomes 2, 2A and 2B respectively for **A** male-specific cross-overs and **B** female-specific cross-overs. Shaded areas represent the 95% confidence interval estimated through bootstrap resampling ($N=100$). Relative physical distance from the telomere was measured from the chromosome ends to centromere boundaries for each p- and q-arm (which were consequently superposed).

Figure S6: LD-based recombination rates around cross-over breakpoints inferred in the pedigree. Line represents the average recombination rate from (18) estimated across 1 kb intervals for 192 cross-overs whose breakpoints are resolved to less than 5 kb.

Figure S7: The effect of the relative likelihood filter threshold on the number of de novo mutation candidates passing filters. Each open circle represents number of de novo mutation candidates that pass the relative likelihood filter threshold (x-axis). The red line indicates the filter value used in this analysis.

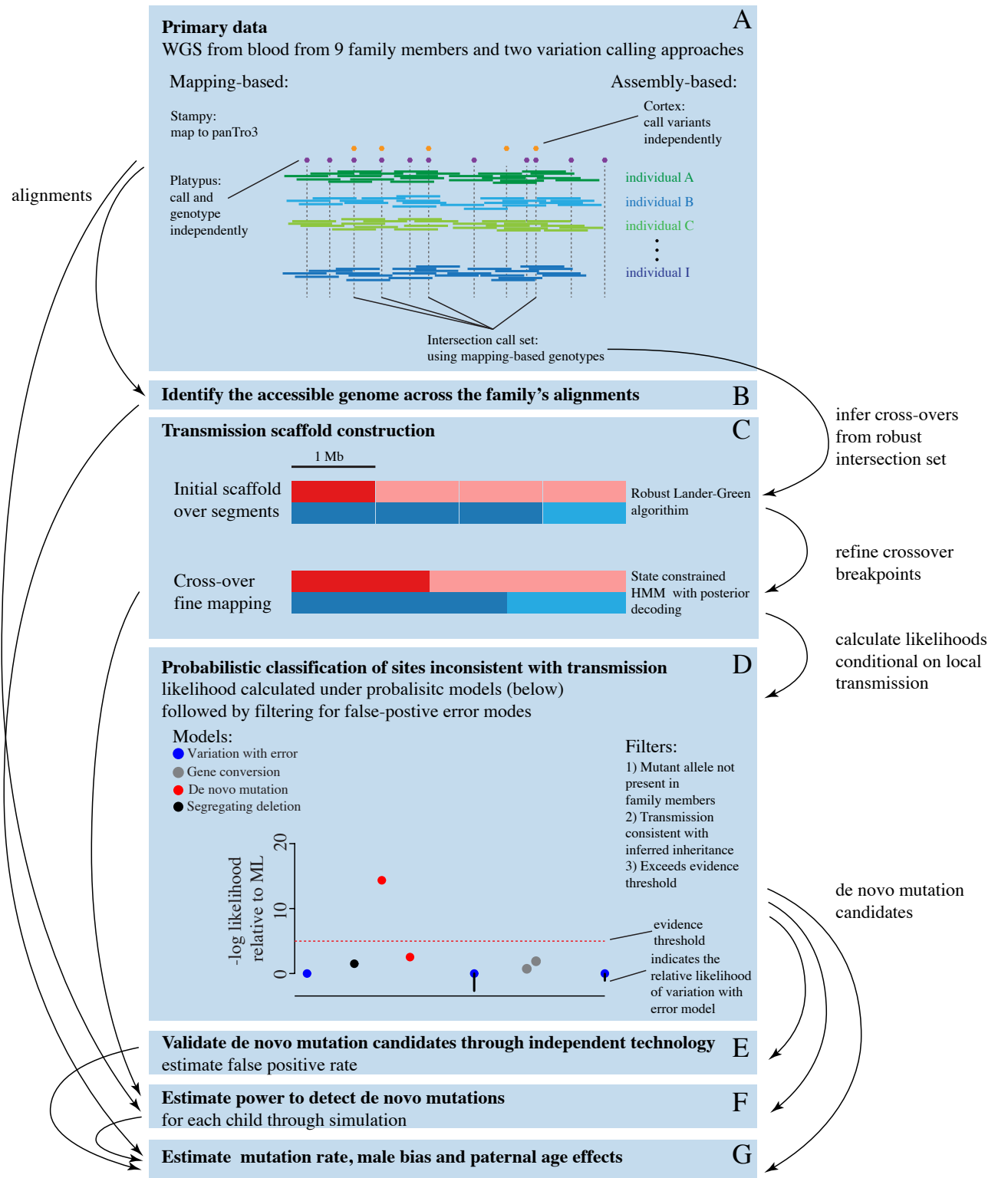
Figure S8: The distribution of de novo mutation events across the autosomes. For each chromosome, represented as grey rectangles, the location of germ line point mutation events are indicated by dots. The child receiving the mutation is distinguished by colour and height above the x-axis. Note stacked events indicate the transmission of events from F (represented by green dots) to children.

Figure S9: The clustering of de novo point mutations within individuals. Points represent the number of clustered point mutations occurring in the same individual for increasing 100 kb distance intervals (red) and the null distribution estimated through permuting the location of mutations (blue, $N=1000$) for **A** all 207 candidate point mutations and **B** the 198 manually curated point mutations. Tick marks represent the 95% confidence intervals for the null distribution.

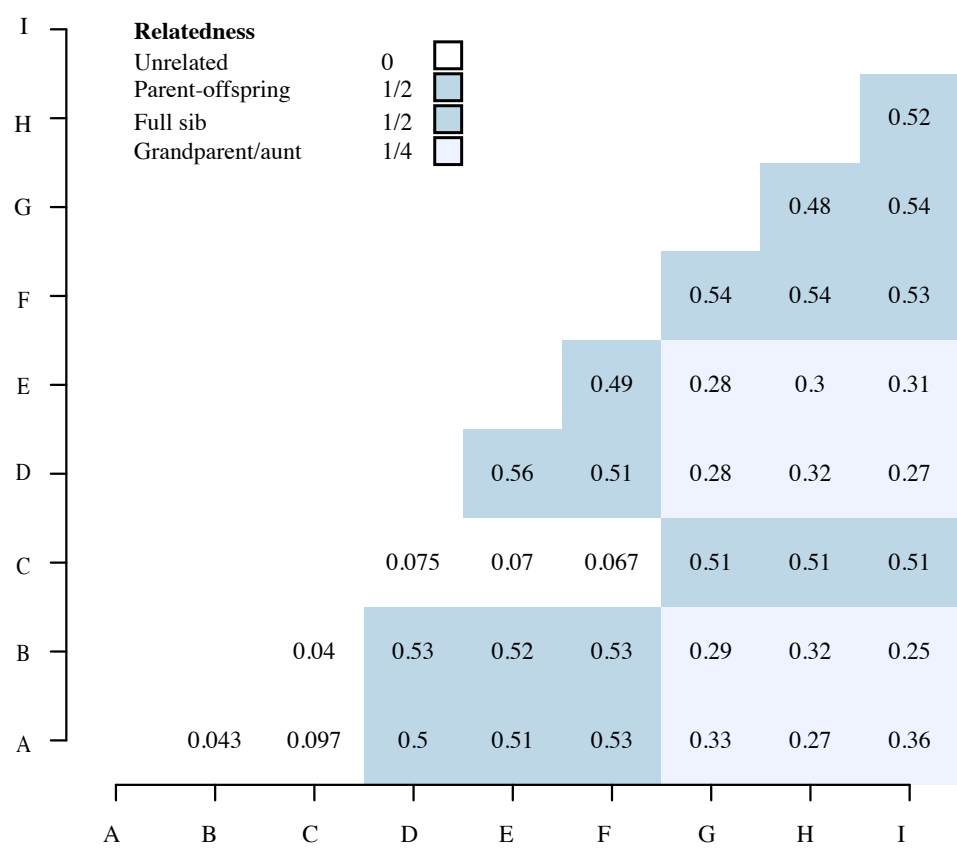
Figure S10: The relationship between de novo mutation events and different genome features. To assess whether the rate of events is affected by sequence context we calculated the distribution of mutation events with distance (red line, i.e. the observed distribution) from **A** repeat elements, **B** gene transcripts, **c** reference assembly gaps. The purple lines represent 100 permutation experiments where events were shifted across chromosomes (see Supplementary text).

Figure S11: The relationship between paternal age effect and the number of de novo mutations stratified by repeat and non-repeat DNA contexts. Points represent paternal age versus the number of point mutations in each child occurring on repeat (black) and non-repeat (red) DNA backgrounds. Linear regression coefficients are shown as dotted lines for events in repeat ($P = 0.119$) and non-repeat ($P = 0.014$). Counts were not corrected for the estimated false-negative rates.

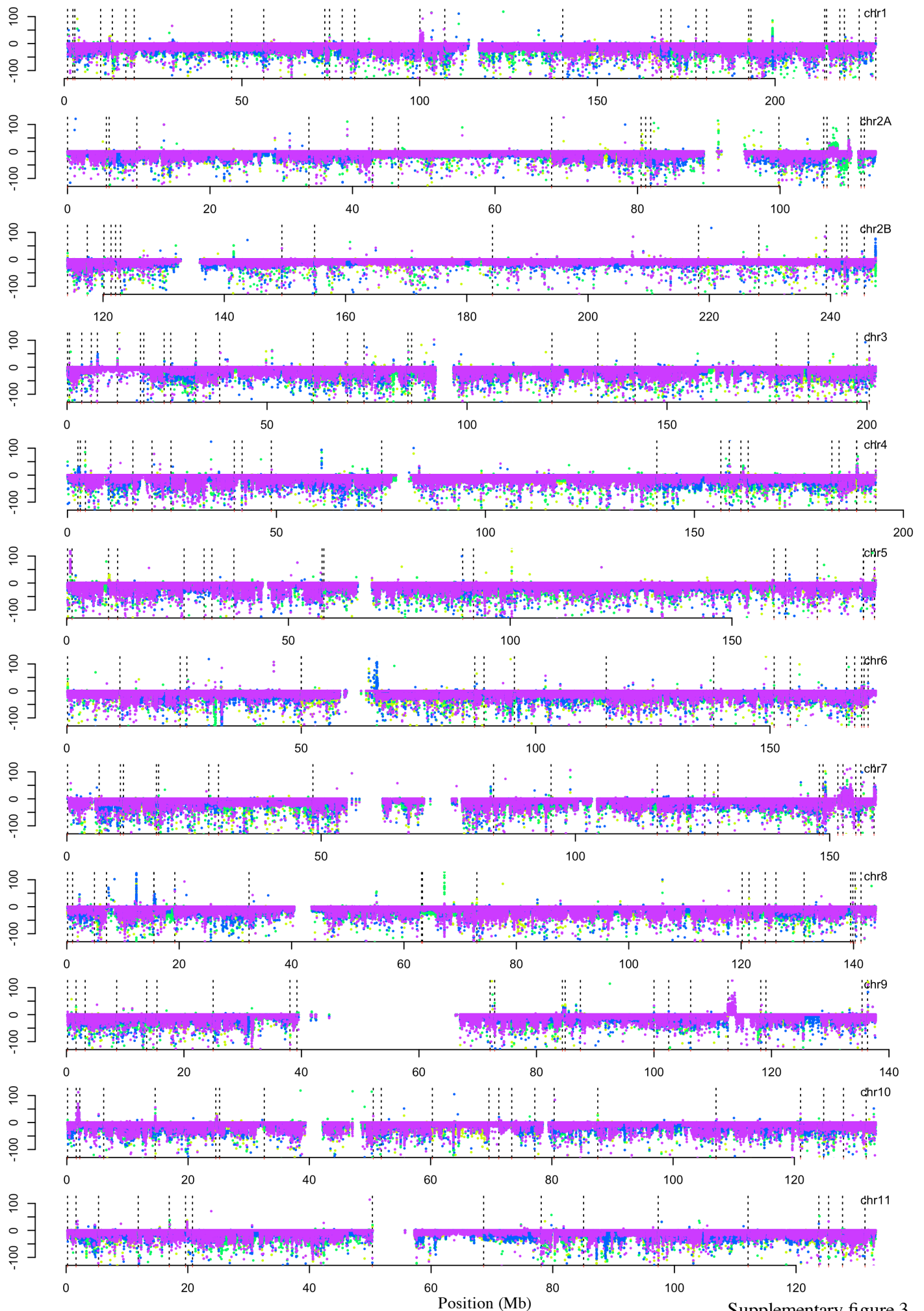
Figure S12: The relationship between paternal and maternal age and the number of de novo point mutations incorporating phase information. The posterior mean estimates for separate paternal (blue) and maternal (red) mutation rates in Western chimpanzees are shown as solid lines with their estimated 95% ETPI envelopes, correcting for the estimated false negative rate in each offspring. Also shown as dotted lines is the estimate from humans for males (blue) and females (red); data from reference 13. Blue and red dots indicate paternal and maternal ages at birth within the pedigree respectively.



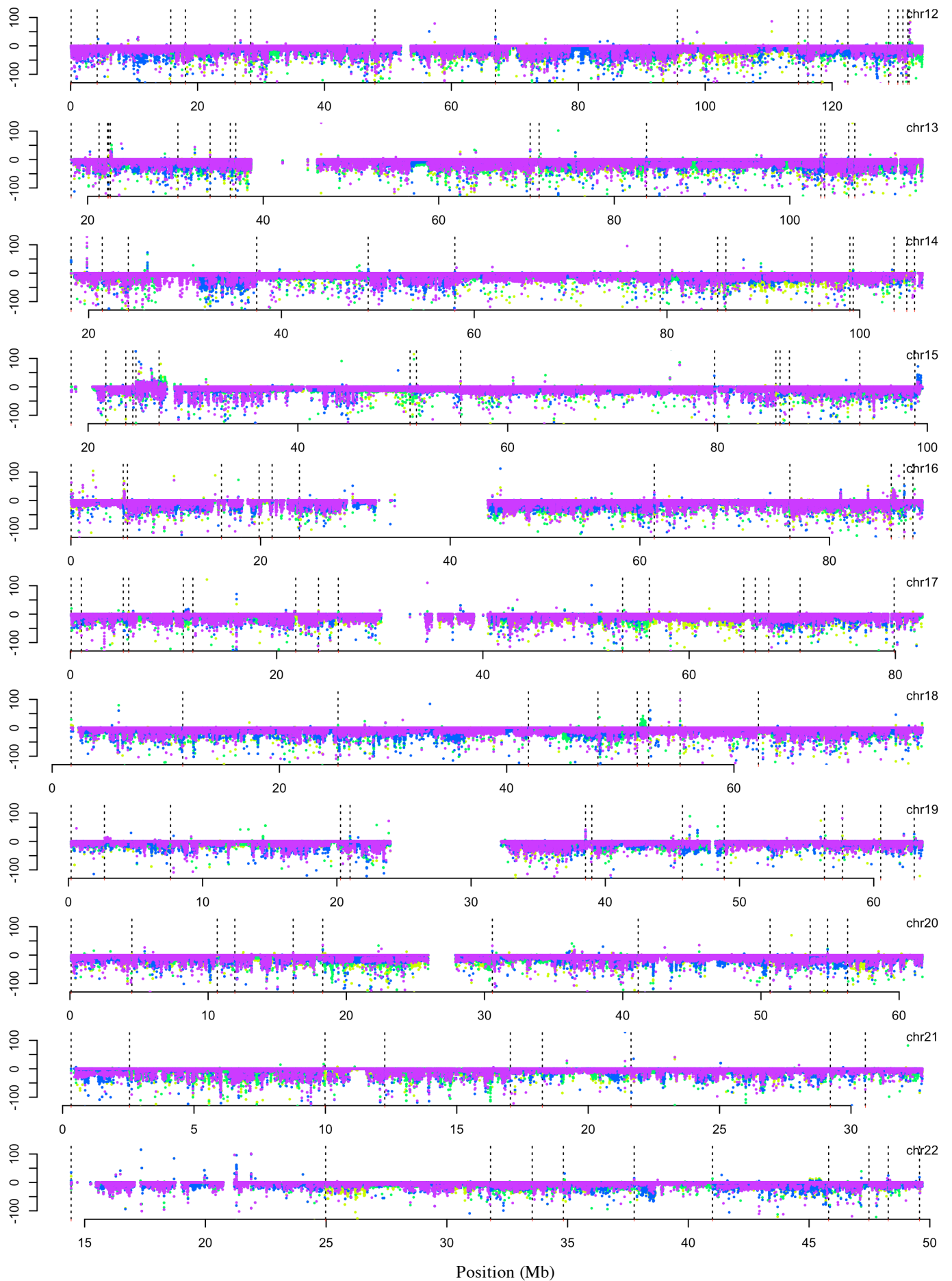
Supplementary figure 1



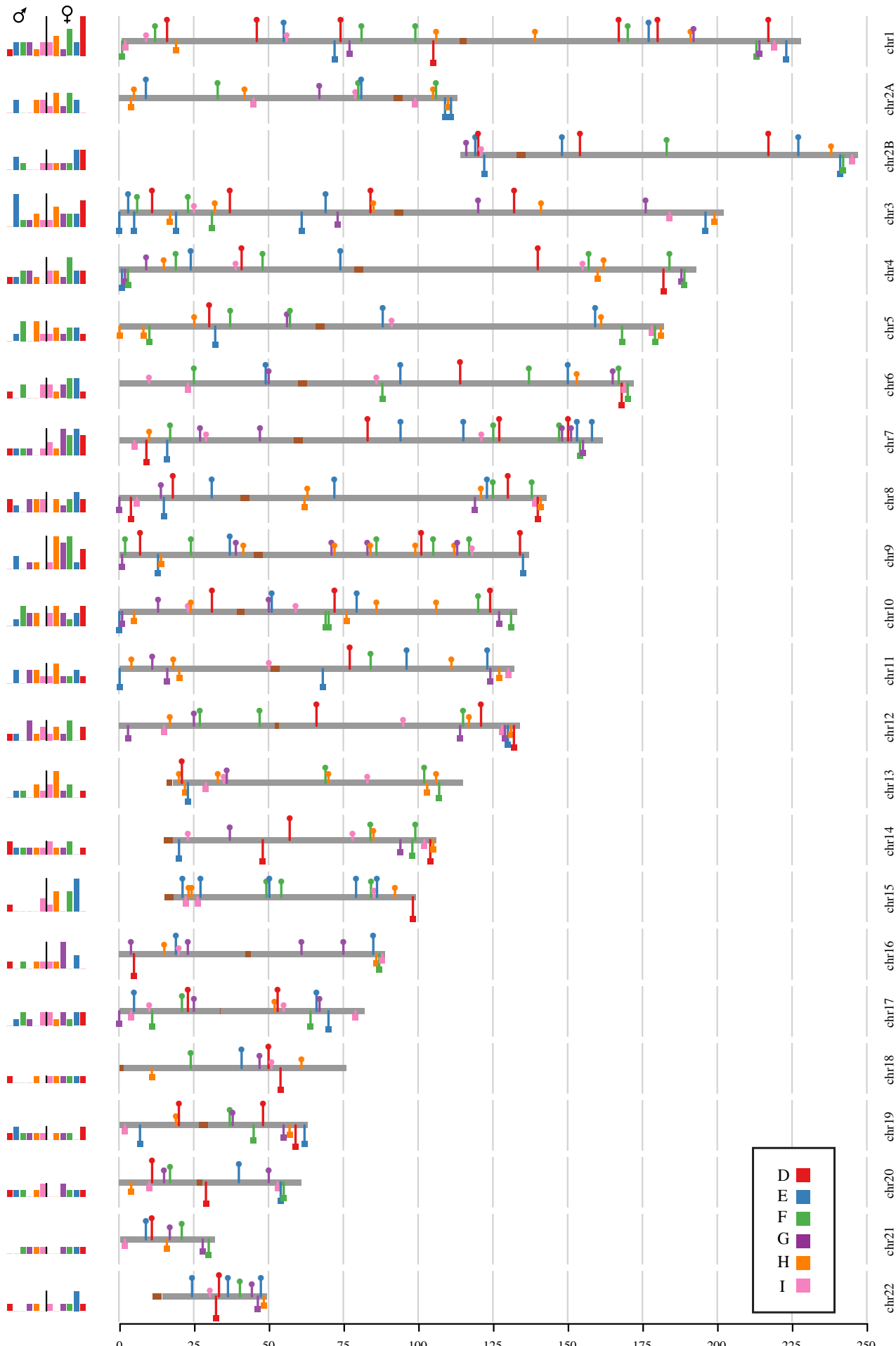
Supplementary figure 2



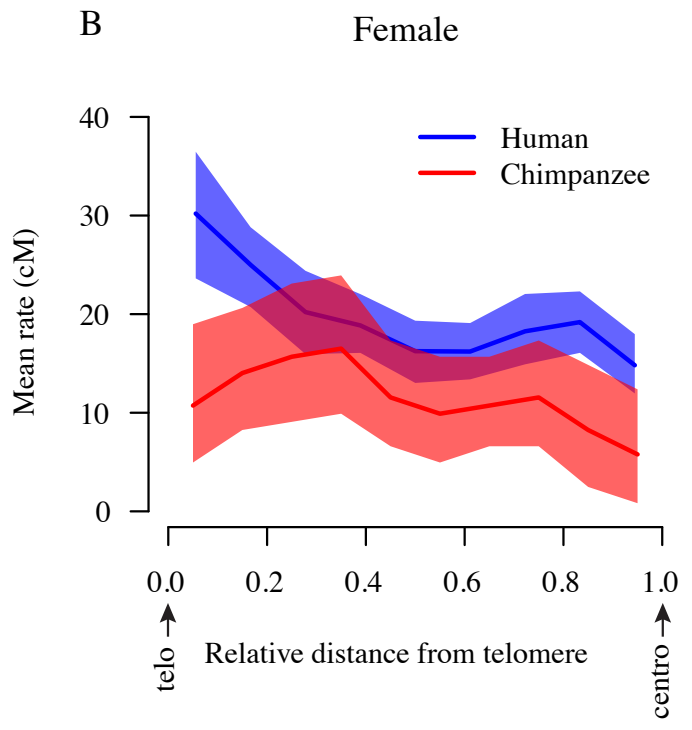
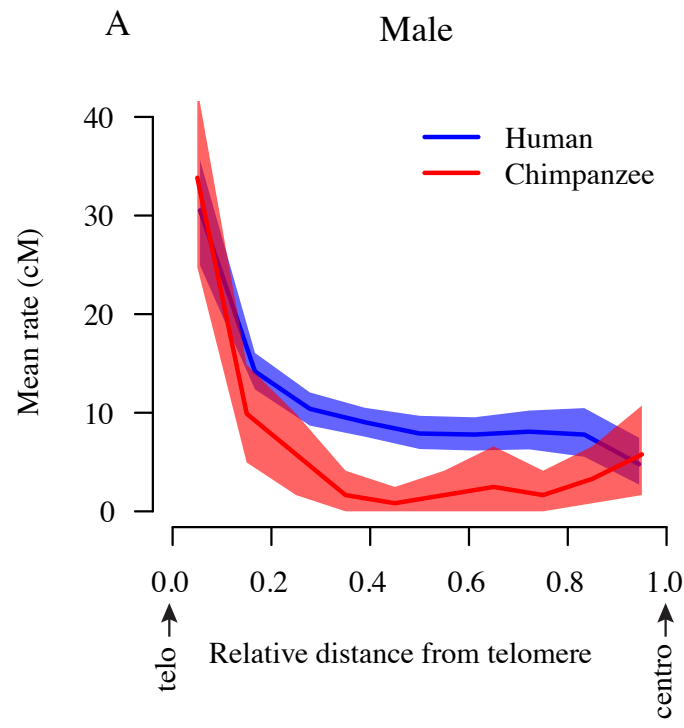
Supplementary figure 3



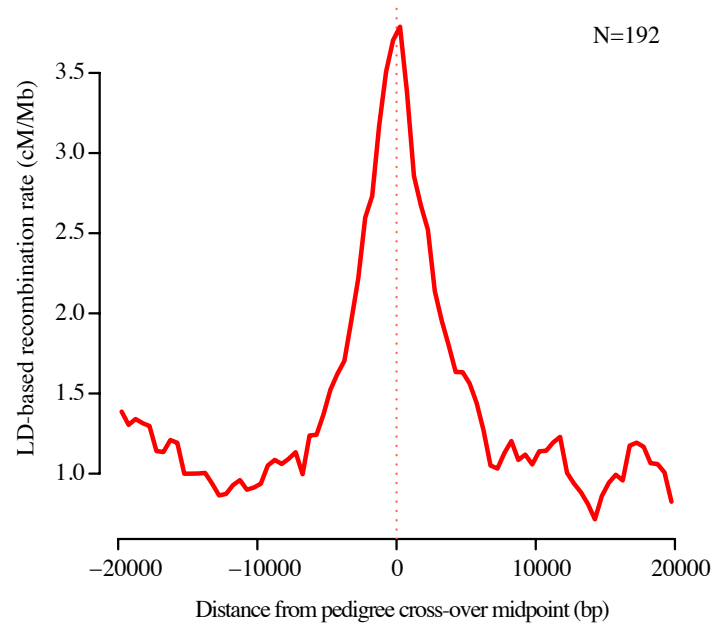
Supplementary figure 3



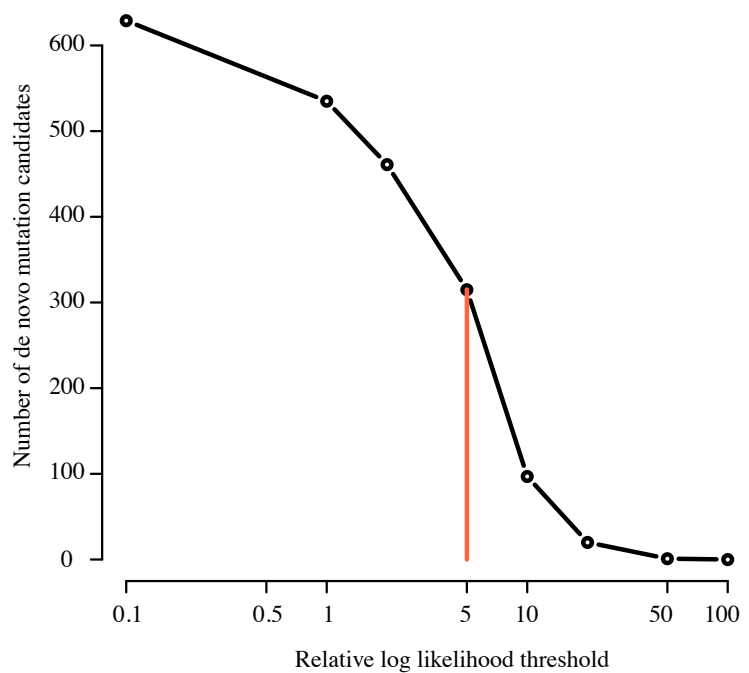
Supplementary figure 4



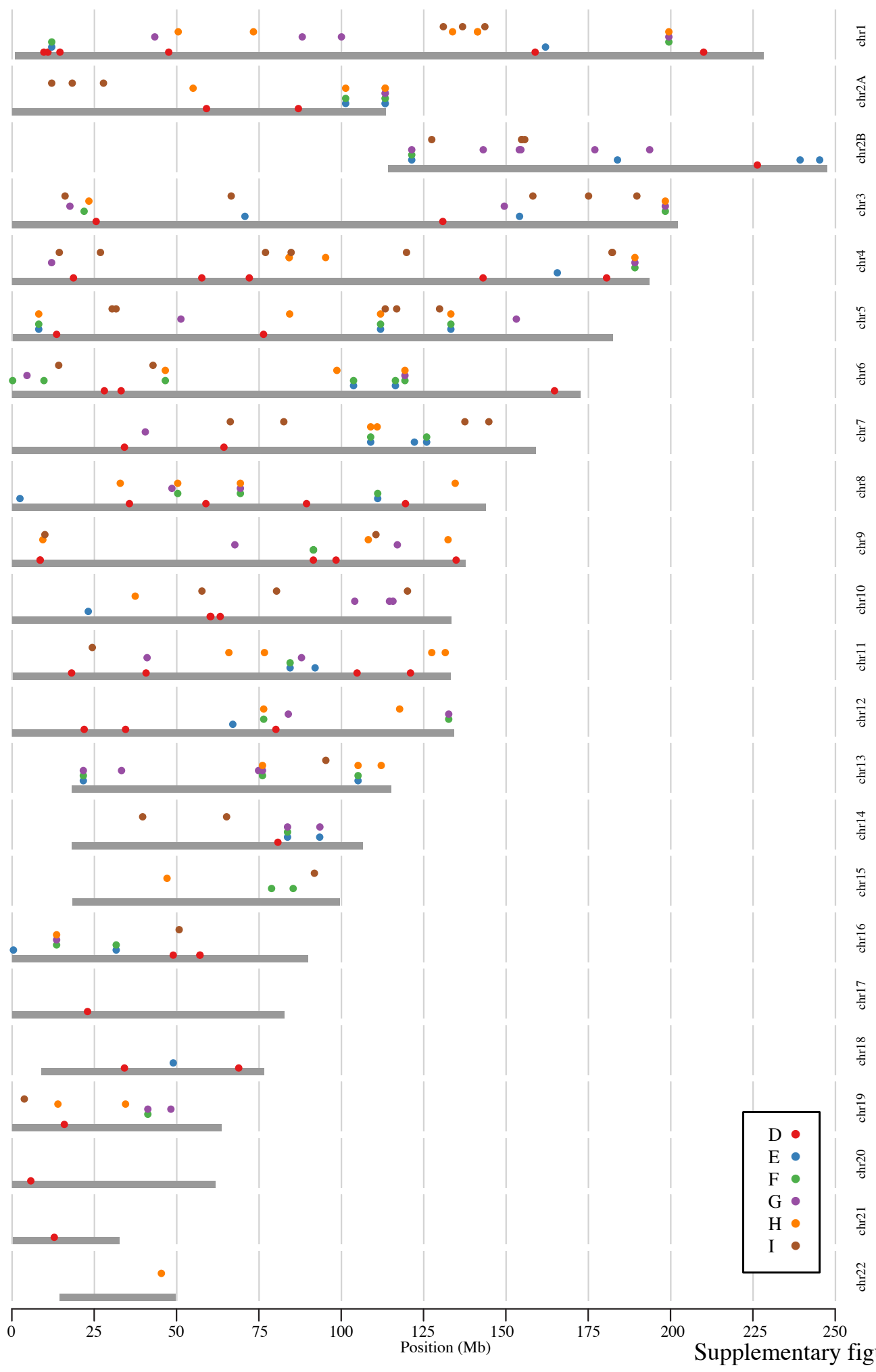
Supplementary figure 5

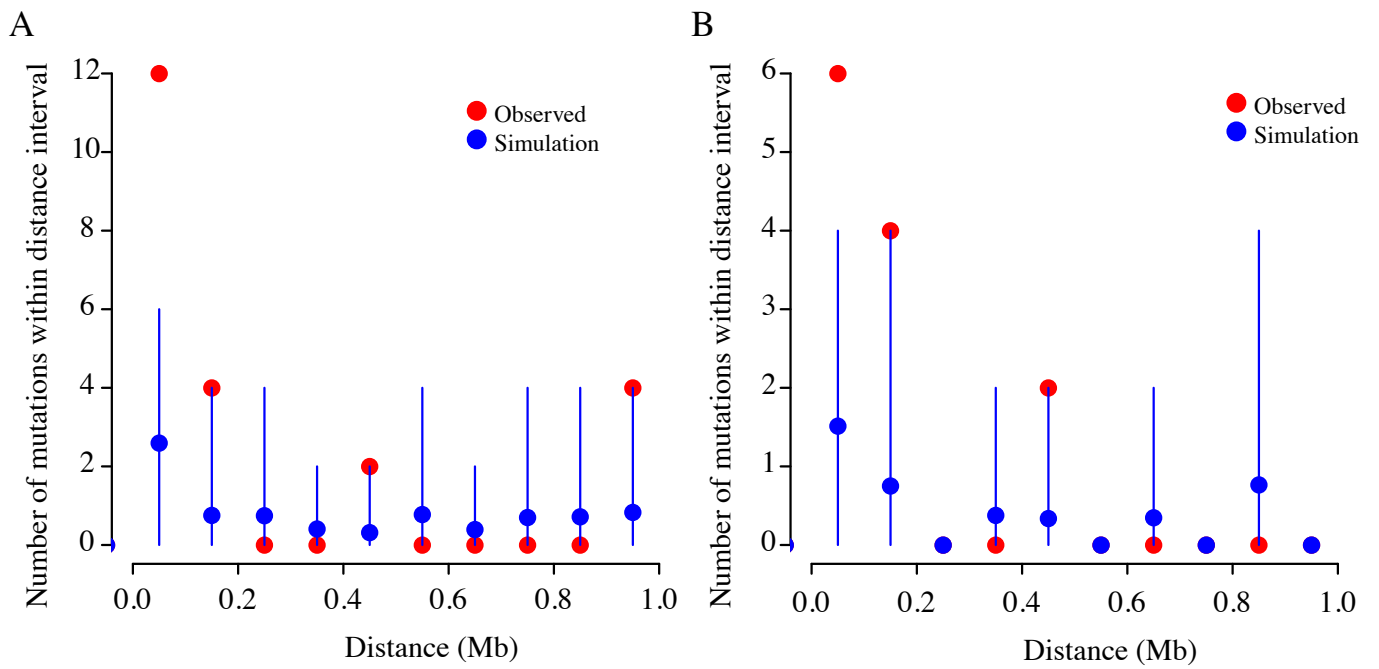


Supplementary figure 6

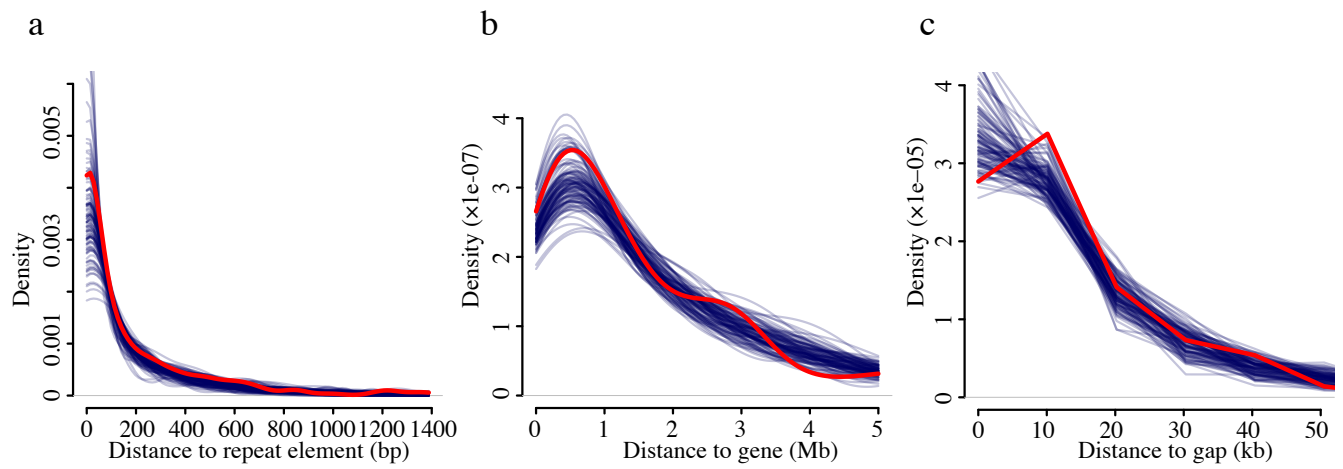


Supplementary figure 7

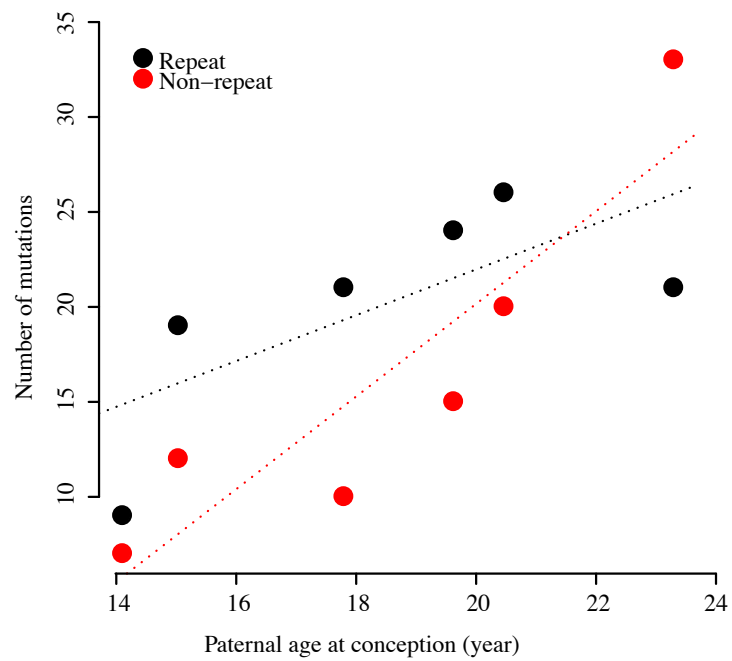




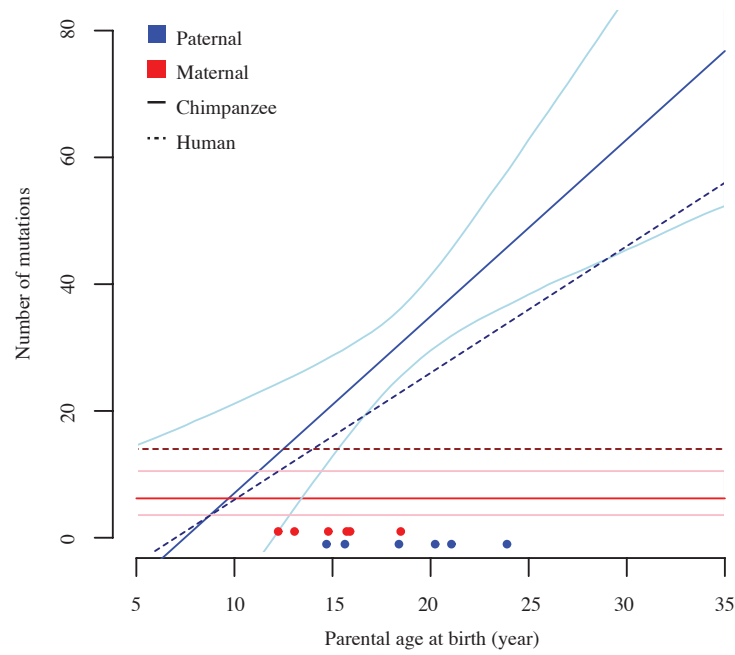
Supplementary figure 9



Supplementary figure 10



Supplementary figure 11



Supplementary figure 12

Table S1: Western chimpanzee pedigree sequencing properties.
 Mapped coverage was calculated after removing PCR duplicates and
 against the panTro3 reference genome.

Individual	Total Sequence (Gb)	Mean coverage	Genome covered by > 15x	# Illumina lanes
A	185.00	63.81	97.80	6
B	166.90	57.54	97.00	5
C	74.20	25.59	87.60	2
D	103.60	35.73	94.70	3
E	66.10	22.78	82.60	2
F	90.20	31.11	94.00	3
G	70.80	24.42	86.00	2
H	72.10	24.85	86.80	2
I	84.90	29.28	90.60	2
Average	101.53	35.01	90.79	

Table S2: Properties of inferred cross-over breakpoints (excluding complex events). Start_bp and End_bp represent the panTro3 coordinates of the 95% credible interval. A 'best-guess' range was calculated as the two consecutive sites with the largest change in the posterior probability.

Chr	Cross-over breakpoint range (95% CI)		Number of sites in 95% CI	Change in posterior probability over cross-over breakpoint range		'Best guess' SNV interval for breakpoint	
	Start (bp)	End (bp)		5' transmission vector	3' transmission vector	Start (bp)	End (bp)
1	2,441,847	2,505,066	41	-0.978	0.976	2,441,847	2,445,577
1	2,995,244	3,006,208	2	-0.998	0.996	3,005,424	3,006,208
1	10,232,552	10,250,285	4	-0.999	0.999	10,240,430	10,250,285
1	13,545,724	13,546,685	1	-1.000	1.000	13,545,724	13,546,685
1	17,341,138	17,394,727	21	-0.999	1.000	17,341,138	17,343,545
1	19,698,531	19,717,500	18	-0.976	0.977	19,703,005	19,703,451
1	47,089,507	47,114,126	19	-1.000	1.000	47,101,077	47,101,905
1	56,125,791	56,169,855	95	-0.966	0.965	56,125,791	56,125,962
1	56,868,170	56,871,573	2	-0.998	0.998	56,868,170	56,871,221
1	73,311,236	73,315,328	4	-0.996	0.996	73,311,236	73,311,412
1	74,660,121	74,666,594	3	-1.000	1.000	74,660,121	74,663,007
1	78,222,576	78,227,450	2	-1.000	1.000	78,222,576	78,227,044
1	81,705,285	81,707,949	4	-1.000	1.000	81,705,285	81,706,090
1	100,068,136	100,075,910	6	-1.000	1.000	100,068,136	100,070,322
1	107,073,526	107,074,796	1	-1.000	1.000	107,073,526	107,074,796
1	140,252,972	140,256,204	4	-1.000	1.000	140,252,972	140,253,601
1	167,949,628	167,953,570	2	-0.999	0.999	167,949,628	167,953,221
1	170,675,861	170,680,617	2	-1.000	0.999	170,675,861	170,680,265
1	177,723,536	177,731,223	7	-1.000	1.000	177,723,536	177,725,185
1	180,727,670	180,755,380	6	-0.987	0.987	180,727,670	180,727,785
1	192,571,877	192,576,000	2	-1.000	1.000	192,573,891	192,576,000
1	193,187,751	193,202,550	9	-0.994	0.994	193,202,355	193,202,550
1	213,951,525	213,962,770	14	-1.000	1.000	213,951,525	213,951,646
1	214,206,657	214,483,663	50	-0.976	0.978	214,482,811	214,483,663
1	218,213,266	218,227,309	4	-1.000	1.000	218,213,266	218,222,220
1	219,495,928	219,504,113	7	-0.999	1.000	219,495,928	219,497,619
1	223,664,146	223,666,641	1	-0.995	0.995	223,664,146	223,666,641
2A	5,455,120	5,500,180	65	-0.970	0.970	5,455,120	5,455,194
2A	5,848,124	5,848,624	1	-0.994	0.994	5,848,124	5,848,624
2A	9,733,226	9,763,261	37	-1.000	1.000	9,733,226	9,734,908
2A	33,887,049	33,889,525	2	-0.999	1.000	33,887,049	33,887,354
2A	42,748,835	42,807,454	32	-0.989	0.998	42,806,619	42,807,454
2A	46,441,412	46,446,273	2	-0.991	0.991	46,441,412	46,443,723
2A	67,765,118	68,011,933	342	-0.977	0.976	67,938,724	67,939,731
2A	80,499,309	80,501,001	3	-0.999	1.000	80,500,839	80,501,001
2A	81,141,703	81,142,893	2	-1.000	1.000	81,141,703	81,141,792
2A	81,843,955	81,845,318	3	-0.974	0.974	81,844,245	81,844,353
2A	99,846,475	99,847,026	2	-0.992	0.992	99,846,475	99,846,579
2A	106,121,023	106,124,492	1	-0.999	0.999	106,121,023	106,124,492
2A	106,593,968	106,604,691	4	-1.000	1.000	106,593,968	106,595,159
2A	109,566,577	109,891,969	315	-1.000	0.999	109,566,577	109,567,536
2A	111,367,877	111,378,240	11	-1.000	0.997	111,367,877	111,369,609
2A	111,830,564	111,911,311	103	-0.962	0.962	111,830,564	111,832,323
2B	117,375,213	117,491,991	113	-0.962	0.964	117,411,338	117,412,620
2B	120,155,683	120,200,849	14	-0.998	0.997	120,155,683	120,157,033
2B	121,323,648	121,339,621	8	-0.999	0.999	121,323,648	121,326,371
2B	122,057,259	122,187,750	75	-0.974	0.971	122,074,976	122,075,171
2B	122,885,204	122,887,334	5	-1.000	1.000	122,885,204	122,885,323
2B	149,506,879	149,508,834	2	-0.995	0.995	149,506,879	149,507,558
2B	154,892,774	154,975,977	93	-0.958	0.958	154,892,774	154,894,868
2B	184,240,584	184,244,092	4	-1.000	1.000	184,240,584	184,242,413
2B	218,229,569	218,233,445	3	-0.993	0.992	218,229,569	218,231,881

2B	228,166,348	228,170,841	4	-0.999	0.999	228,166,348	228,166,621
2B	239,288,386	239,292,244	5	-0.982	0.982	239,291,940	239,292,244
2B	241,849,147	242,015,635	295	-0.978	0.980	241,883,308	241,883,894
2B	242,679,190	242,693,766	13	-1.000	1.000	242,679,190	242,683,038
2B	245,576,136	245,669,053	139	-0.969	0.968	245,577,219	245,577,989
3	591,750	599,839	2	-1.000	0.999	591,750	594,013
3	3,664,956	3,674,874	9	-1.000	1.000	3,664,956	3,665,506
3	6,002,789	6,567,761	580	-0.966	0.978	6,060,086	6,061,550
3	7,574,910	7,577,089	5	-0.989	1.000	7,575,992	7,577,089
3	12,573,323	12,574,457	2	-0.995	0.997	12,574,342	12,574,457
3	16,592,674	18,556,475	1590	-0.976	0.975	18,354,301	18,356,435
3	19,185,789	20,556,385	1340	-0.967	0.967	19,185,789	19,186,542
3	24,267,410	24,488,634	210	-0.961	0.961	24,267,410	24,267,461
3	25,915,083	25,917,107	1	-0.977	0.977	25,915,083	25,917,107
3	32,179,221	32,259,319	77	-0.999	0.997	32,179,221	32,179,532
3	38,160,246	38,161,480	2	-0.998	0.998	38,160,246	38,161,008
3	61,570,730	61,575,636	8	-0.998	0.998	61,570,730	61,571,648
3	70,118,927	70,124,622	2	-0.987	0.988	70,118,927	70,120,798
3	74,244,857	74,252,179	22	-0.999	1.000	74,245,958	74,245,999
3	85,227,579	85,234,887	3	-0.997	0.997	85,227,579	85,234,065
3	86,148,266	86,564,337	347	-0.962	0.967	86,148,266	86,148,297
3	121,237,846	121,238,918	1	-0.988	0.988	121,237,846	121,238,918
3	132,703,955	132,985,912	159	-0.975	0.960	132,703,955	132,705,246
3	142,024,302	142,033,075	4	-0.998	0.998	142,031,085	142,033,075
3	177,291,534	177,292,847	4	-0.998	0.998	177,292,372	177,292,847
3	185,348,130	185,361,895	6	-0.994	0.993	185,348,130	185,349,449
3	197,508,910	197,520,026	8	-0.978	0.978	197,516,831	197,517,417
3	200,569,370	200,578,128	3	-0.998	0.998	200,569,370	200,569,687
4	2,500,770	2,507,786	4	-0.998	0.998	2,500,770	2,501,514
4	3,089,615	3,103,452	4	-0.999	0.999	3,089,615	3,090,230
4	4,298,295	4,301,190	3	-1.000	1.000	4,298,295	4,299,514
4	10,354,453	10,367,367	4	-0.978	0.978	10,366,254	10,367,367
4	15,663,521	15,688,189	3	-0.978	0.978	15,663,521	15,677,192
4	20,229,292	20,247,432	9	-1.000	1.000	20,229,292	20,229,516
4	24,718,463	24,856,347	210	-0.976	0.975	24,775,244	24,776,150
4	39,665,542	40,467,976	449	-0.974	0.967	39,913,017	39,916,859
4	41,781,860	41,785,929	1	-1.000	1.000	41,781,860	41,785,929
4	48,773,524	48,817,372	52	-0.963	0.963	48,773,524	48,775,085
4	75,178,722	75,186,828	8	-0.979	0.979	75,178,722	75,179,195
4	141,008,512	141,014,993	15	-0.998	0.998	141,008,512	141,008,719
4	156,323,245	156,333,670	5	-0.998	0.999	156,331,080	156,333,670
4	158,337,336	158,341,381	1	-1.000	1.000	158,337,336	158,341,381
4	161,108,122	161,132,435	21	-0.998	1.000	161,118,934	161,120,248
4	162,865,294	162,943,956	30	-1.000	1.000	162,865,294	162,870,491
4	182,892,346	182,894,453	3	-1.000	1.000	182,892,346	182,892,709
4	184,610,507	184,613,308	2	-1.000	1.000	184,610,507	184,612,326
4	188,814,505	189,494,515	662	-0.999	0.975	188,814,505	188,814,869
4	188,828,730	189,982,900	1102	-0.993	0.977	188,828,730	188,831,679
5	1,207,806	1,227,381	24	-0.980	0.981	1,216,819	1,216,891
5	9,435,698	9,675,237	183	-0.996	1.000	9,435,698	9,441,227
5	11,484,840	11,492,310	7	-1.000	1.000	11,484,840	11,485,372
5	26,469,132	26,489,893	23	-0.999	0.991	26,472,906	26,473,860
5	30,983,042	30,984,782	1	-0.999	0.999	30,983,042	30,984,782
5	32,738,776	33,020,902	232	-0.964	0.964	32,744,478	32,746,008
5	37,697,810	37,698,911	2	-1.000	1.000	37,697,810	37,698,828
5	57,578,570	57,583,039	3	-0.994	0.994	57,580,750	57,583,039
5	57,991,361	57,993,707	2	-1.000	1.000	57,991,361	57,993,641
5	89,288,464	89,300,483	7	-1.000	1.000	89,288,464	89,288,953
5	91,723,109	91,725,227	1	-0.999	0.999	91,723,109	91,725,227
5	159,475,021	159,856,976	345	-0.978	0.970	159,475,021	159,477,274
5	162,106,063	162,108,625	4	-0.996	0.997	162,108,514	162,108,625
5	169,241,432	169,258,577	8	-0.994	0.992	169,241,432	169,245,488

5	179,608,944	179,612,841	7	-0.976	0.976	179,608,944	179,608,986
5	179,682,248	179,701,293	32	-1.000	1.000	179,682,248	179,682,378
5	182,141,565	182,144,226	1	-1.000	1.000	182,141,565	182,144,226
6	11,280,722	11,308,816	38	-0.997	0.999	11,307,354	11,308,816
6	24,171,606	24,188,963	11	-0.996	0.996	24,171,606	24,176,223
6	25,590,757	25,591,956	3	-1.000	1.000	25,590,757	25,591,148
6	49,982,712	49,985,257	5	-0.999	0.999	49,982,712	49,983,017
6	50,019,651	50,025,220	6	-1.000	1.000	50,019,651	50,021,033
6	87,013,116	87,015,061	4	-1.000	1.000	87,013,116	87,013,231
6	88,992,489	89,001,287	4	-0.997	0.996	88,992,489	88,993,665
6	95,469,655	95,485,337	7	-1.000	1.000	95,469,655	95,470,265
6	115,064,540	115,068,904	2	-1.000	1.000	115,064,540	115,067,571
6	137,998,852	138,016,767	9	-0.999	0.999	137,998,852	138,002,791
6	150,889,020	150,892,950	4	-0.996	0.996	150,889,020	150,891,772
6	154,338,020	154,358,157	4	-0.996	0.996	154,352,405	154,358,157
6	166,338,755	166,343,442	3	-0.997	0.997	166,338,755	166,342,194
6	168,070,094	168,082,178	7	-1.000	1.000	168,070,094	168,071,497
6	169,556,636	169,556,711	1	-0.999	0.999	169,556,636	169,556,711
6	170,073,085	170,078,301	1	-0.994	0.994	170,073,085	170,078,301
6	170,724,621	171,543,928	741	-0.977	0.976	170,941,291	170,942,186
7	6,348,527	6,352,997	9	-1.000	1.000	6,349,119	6,350,365
7	10,518,784	10,525,782	22	-1.000	1.000	10,518,784	10,518,838
7	11,118,540	11,124,248	4	-0.999	0.999	11,123,929	11,124,248
7	17,610,007	17,620,761	6	-1.000	1.000	17,610,007	17,610,755
7	18,024,956	18,187,484	286	-0.966	0.967	18,048,551	18,049,586
7	27,898,891	27,904,612	2	-0.994	0.994	27,898,891	27,900,811
7	29,814,810	29,857,164	27	-1.000	1.000	29,814,810	29,816,242
7	48,381,636	48,385,193	2	-1.000	1.000	48,382,039	48,385,193
7	83,908,479	83,913,525	4	-1.000	1.000	83,908,479	83,911,625
7	95,211,027	95,217,794	12	-0.995	0.995	95,211,027	95,211,094
7	116,110,106	116,133,811	10	-1.000	1.000	116,110,106	116,110,387
7	122,192,431	122,194,741	4	-0.999	0.999	122,192,431	122,192,646
7	125,330,999	126,607,072	1277	-0.975	0.978	125,452,698	125,455,673
7	126,632,267	128,599,126	1953	-0.976	0.977	128,023,685	128,024,122
7	147,977,909	147,978,614	1	-1.000	1.000	147,977,909	147,978,614
7	148,707,594	148,709,325	1	-0.997	0.997	148,707,594	148,709,325
7	151,615,969	151,618,325	3	-1.000	1.000	151,615,969	151,617,049
7	152,625,222	154,462,036	1796	-1.000	1.000	152,625,222	152,625,531
7	155,141,874	155,225,328	5	-0.999	1.000	155,141,874	155,143,159
7	156,128,902	156,141,973	44	-1.000	0.994	156,128,902	156,129,105
7	158,724,978	159,504,421	346	-0.997	0.999	158,724,978	158,725,451
8	986,839	1,030,283	52	-0.977	0.979	1,029,306	1,030,283
8	4,919,749	4,923,013	3	-0.999	0.999	4,919,749	4,920,055
8	6,967,967	7,471,114	57	-0.994	0.994	7,065,104	7,071,705
8	15,499,679	15,501,791	3	-1.000	1.000	15,499,679	15,500,504
8	15,510,115	15,878,897	441	-1.000	0.999	15,510,115	15,510,176
8	19,222,264	19,337,976	101	-0.960	0.960	19,222,264	19,222,412
8	32,422,762	32,433,044	8	-0.982	0.983	32,432,277	32,432,595
8	63,141,750	63,145,920	1	-1.000	1.000	63,141,750	63,145,920
8	63,290,289	63,291,205	1	-0.995	0.995	63,290,289	63,291,205
8	72,975,276	73,013,850	6	-1.000	1.000	72,975,276	72,977,861
8	120,149,417	120,187,411	28	-0.998	0.998	120,186,150	120,187,411
8	121,409,215	121,410,736	2	-0.984	0.983	121,409,215	121,409,801
8	124,290,396	124,294,306	4	-1.000	1.000	124,290,396	124,292,755
8	126,193,232	126,197,187	3	-1.000	1.000	126,193,232	126,194,835
8	131,206,217	131,209,574	4	-1.000	1.000	131,206,217	131,206,365
8	139,474,158	139,500,818	3	-0.996	0.997	139,474,158	139,500,458
8	139,879,142	139,900,186	14	-1.000	1.000	139,879,142	139,885,625
8	140,298,573	140,305,002	5	-1.000	1.000	140,298,573	140,301,933
8	141,347,153	141,354,119	2	-0.986	0.986	141,347,153	141,353,714
9	1,630,657	1,632,255	4	-0.991	0.992	1,630,657	1,630,996
9	3,185,761	3,192,754	2	-1.000	1.000	3,185,761	3,190,995

9	8,547,633	8,552,723	4	-1.000	1.000	8,547,633	8,550,262
9	13,650,075	13,665,508	16	-0.981	0.981	13,650,075	13,652,525
9	15,412,781	15,421,385	6	-0.990	0.991	15,412,781	15,414,318
9	24,968,658	24,973,175	2	-0.999	0.999	24,968,658	24,973,001
9	38,037,339	38,047,730	6	-1.000	1.000	38,037,339	38,038,446
9	39,233,243	39,251,670	19	-1.000	1.000	39,233,243	39,245,318
9	72,105,270	72,119,751	8	-0.978	0.977	72,105,270	72,105,818
9	72,880,818	72,881,965	1	-0.997	0.997	72,880,818	72,881,965
9	84,405,173	84,553,033	42	-0.954	0.954	84,405,173	84,405,780
9	84,485,350	85,071,626	257	-0.976	0.978	85,069,351	85,071,626
9	87,478,946	87,485,326	5	-0.993	0.993	87,478,946	87,482,721
9	100,004,771	100,005,957	1	-1.000	1.000	100,004,771	100,005,957
9	102,514,218	102,518,009	2	-1.000	1.000	102,514,218	102,515,853
9	106,248,206	106,254,268	4	-1.000	1.000	106,248,206	106,248,801
9	111,564,592	113,535,279	1769	-0.977	0.976	112,601,613	112,606,051
9	112,561,842	114,326,330	1553	-1.000	0.978	112,561,842	112,562,684
9	118,179,365	118,180,446	1	-1.000	1.000	118,179,365	118,180,446
9	119,054,671	119,055,135	1	-0.998	0.998	119,054,671	119,055,135
9	135,425,172	135,431,122	9	-0.979	0.979	135,425,172	135,426,412
9	136,358,512	136,398,419	17	-0.996	0.996	136,358,512	136,366,092
10	1,550,828	1,570,130	10	-1.000	1.000	1,550,828	1,556,164
10	2,095,159	2,142,015	75	-0.963	0.962	2,142,006	2,142,015
10	6,080,764	6,082,588	2	-0.997	0.997	6,080,764	6,082,529
10	14,568,985	14,569,761	2	-1.000	1.000	14,569,750	14,569,761
10	24,570,527	24,573,942	2	-1.000	1.000	24,573,321	24,573,942
10	25,196,003	25,199,949	7	-1.000	1.000	25,196,003	25,197,292
10	32,567,348	32,575,395	5	-1.000	1.000	32,567,348	32,568,159
10	50,544,017	50,544,339	1	-0.997	0.997	50,544,017	50,544,339
10	51,866,159	51,867,113	2	-0.999	0.999	51,866,159	51,866,958
10	60,290,608	60,302,988	10	-1.000	1.000	60,293,054	60,294,194
10	69,633,400	70,566,132	890	-0.969	0.969	69,633,697	69,638,220
10	70,918,199	71,533,704	326	-0.966	0.966	71,260,580	71,271,582
10	71,596,405	73,473,633	761	-0.978	0.975	73,421,810	73,422,586
10	77,188,862	77,190,553	3	-0.985	0.985	77,188,862	77,189,761
10	80,374,734	80,377,416	1	-0.999	0.999	80,374,734	80,377,416
10	87,574,089	87,574,122	1	-0.989	0.989	87,574,089	87,574,122
10	107,082,724	107,085,601	3	-1.000	1.000	107,082,724	107,082,969
10	121,019,435	121,035,196	21	-1.000	1.000	121,019,435	121,021,259
10	124,841,359	124,849,049	10	-1.000	1.000	124,841,359	124,841,676
10	128,110,535	128,121,899	8	-0.998	1.000	128,112,828	128,114,799
10	131,844,159	131,847,627	2	-1.000	1.000	131,844,159	131,847,244
11	1,628,694	1,640,720	2	-0.996	0.996	1,628,694	1,637,294
11	5,327,400	5,332,510	4	-0.982	0.982	5,327,400	5,327,766
11	11,850,457	11,851,616	2	-0.997	0.997	11,850,782	11,851,616
11	16,946,887	16,953,966	5	-0.997	0.997	16,948,707	16,948,997
11	19,630,509	19,639,213	6	-0.995	0.995	19,630,509	19,630,788
11	20,776,287	20,777,212	1	-0.976	0.976	20,776,287	20,777,212
11	50,342,265	50,362,743	4	-1.000	1.000	50,350,914	50,362,743
11	68,637,033	68,641,770	1	-0.983	0.983	68,637,033	68,641,770
11	78,104,016	78,105,320	1	-0.999	0.999	78,104,016	78,105,320
11	85,074,016	85,074,353	1	-1.000	1.000	85,074,016	85,074,353
11	97,336,887	97,338,397	1	-0.995	0.995	97,336,887	97,338,397
11	112,109,174	112,114,033	4	-1.000	1.000	112,109,174	112,111,226
11	123,752,898	123,753,678	1	-0.997	0.997	123,752,898	123,753,678
11	125,355,248	125,372,269	14	-1.000	0.996	125,355,248	125,355,448
11	127,644,015	127,647,225	6	-1.000	1.000	127,644,015	127,644,977
11	131,324,185	131,334,934	14	-0.998	0.999	131,334,632	131,334,934
12	4,180,102	4,182,105	1	-0.985	0.985	4,180,102	4,182,105
12	15,774,545	15,777,073	2	-0.996	0.996	15,774,545	15,776,103
12	18,094,718	18,097,239	2	-0.999	0.999	18,094,718	18,095,370
12	25,910,632	25,924,647	1	-0.996	0.996	25,910,632	25,924,647
12	28,370,026	28,372,830	2	-0.987	0.986	28,370,026	28,371,507

12	47,957,583	47,961,545	2	-1.000	1.000	47,957,583	47,958,784
12	66,947,512	66,953,217	2	-1.000	1.000	66,947,512	66,952,973
12	95,614,649	95,616,866	1	-0.999	0.999	95,614,649	95,616,866
12	114,699,794	114,836,494	146	-0.967	0.962	114,699,794	114,701,048
12	116,185,494	116,188,813	1	-0.992	0.992	116,185,494	116,188,813
12	118,279,231	118,290,508	3	-0.968	0.968	118,289,910	118,290,508
12	122,493,091	122,529,899	12	-0.983	0.983	122,493,091	122,493,701
12	128,913,891	128,928,060	5	-0.999	0.999	128,926,781	128,928,060
12	130,360,229	130,374,202	12	-1.000	1.000	130,360,229	130,363,001
12	131,161,351	131,166,882	4	-0.998	0.998	131,161,351	131,162,265
12	131,929,345	131,935,511	5	-0.988	0.988	131,929,345	131,929,484
12	132,126,689	132,250,526	48	-0.958	0.958	132,126,689	132,127,813
13	21,303,955	21,306,162	2	-0.991	0.991	21,303,955	21,304,218
13	22,262,931	22,280,126	13	-1.000	1.000	22,262,931	22,263,066
13	22,395,101	22,426,767	11	-1.000	1.000	22,395,101	22,396,003
13	22,583,790	22,716,640	168	-0.999	0.999	22,583,790	22,585,337
13	30,283,145	30,305,683	14	-1.000	1.000	30,283,145	30,287,102
13	33,796,020	34,073,185	261	-0.976	0.975	33,952,204	33,955,121
13	36,248,915	36,249,663	2	-0.999	0.999	36,248,915	36,249,219
13	36,872,783	36,880,639	3	-0.996	0.996	36,872,783	36,875,145
13	70,421,599	70,422,544	2	-1.000	1.000	70,421,599	70,422,096
13	71,439,829	71,448,385	4	-0.996	0.996	71,439,829	71,444,213
13	83,670,502	83,683,804	6	-0.992	0.990	83,670,502	83,674,431
13	103,542,652	103,543,465	1	-1.000	1.000	103,542,652	103,543,465
13	103,974,684	103,978,881	6	-0.999	0.998	103,974,684	103,975,047
13	106,713,059	106,716,421	4	-0.998	0.998	106,715,494	106,716,421
13	107,410,781	107,421,913	7	-0.990	0.990	107,410,781	107,411,080
14	21,417,432	21,419,074	2	-0.994	0.994	21,417,432	21,418,964
14	24,110,324	24,119,076	5	-1.000	1.000	24,118,025	24,119,076
14	37,436,483	37,450,131	3	-0.995	0.995	37,437,723	37,450,131
14	49,000,662	49,010,576	10	-0.998	0.998	49,000,662	49,001,752
14	57,997,106	57,998,548	1	-1.000	1.000	57,997,106	57,998,548
14	79,296,411	79,334,909	30	-0.999	0.999	79,296,411	79,296,491
14	85,259,381	85,312,417	66	-0.970	0.970	85,259,381	85,259,546
14	86,114,011	86,131,903	11	-0.983	0.983	86,114,011	86,115,268
14	95,043,537	95,057,965	14	-0.998	0.998	95,043,537	95,050,747
14	98,975,276	98,982,594	3	-1.000	1.000	98,975,276	98,975,956
14	99,319,164	99,324,279	8	-1.000	1.000	99,319,164	99,319,497
14	103,562,145	103,565,978	2	-1.000	1.000	103,562,145	103,563,824
14	104,878,950	104,908,741	14	-0.997	0.973	104,879,756	104,883,375
14	105,696,342	106,073,865	8	-0.989	0.988	105,696,342	105,696,442
15	21,711,253	21,823,866	5	-0.999	0.999	21,711,253	21,711,308
15	23,594,695	23,596,739	3	-0.998	0.999	23,596,163	23,596,739
15	24,264,401	24,265,361	2	-0.995	0.995	24,264,401	24,264,433
15	24,562,663	25,760,679	1255	-1.000	1.000	24,567,412	24,569,016
15	26,768,065	28,268,032	657	-1.000	1.000	26,768,065	26,768,543
15	50,694,698	50,699,905	5	-1.000	1.000	50,694,698	50,695,125
15	51,302,142	51,302,235	1	-0.997	0.997	51,302,142	51,302,235
15	55,513,899	55,518,680	1	-1.000	1.000	55,513,899	55,518,680
15	79,724,888	79,736,648	1	-1.000	1.000	79,724,888	79,736,648
15	85,564,910	85,571,575	2	-1.000	1.000	85,564,910	85,570,701
15	85,966,499	85,980,375	17	-0.998	0.998	85,966,499	85,968,201
15	86,858,229	86,866,038	1	-0.964	0.964	86,858,229	86,866,038
15	93,564,445	93,573,691	4	-1.000	1.000	93,570,581	93,572,961
15	98,818,827	98,822,189	2	-0.994	0.994	98,818,827	98,821,952
16	5,504,705	5,516,929	9	-1.000	1.000	5,515,494	5,516,929
16	5,963,271	6,079,635	218	-0.979	0.975	5,963,271	5,963,583
16	15,870,897	15,883,685	6	-0.991	0.994	15,878,790	15,883,685
16	19,851,052	19,857,413	8	-0.986	0.985	19,851,052	19,851,464
16	21,219,984	21,292,281	6	-0.998	0.999	21,219,984	21,220,717
16	24,101,033	24,102,096	1	-1.000	1.000	24,101,033	24,102,096
16	61,521,752	61,522,839	2	-1.000	0.999	61,521,752	61,521,759

16	75,816,898	75,826,704	14	-0.999	0.999	75,821,970	75,823,276
16	86,506,963	86,519,459	16	-1.000	1.000	86,506,963	86,507,557
16	86,517,647	86,977,729	574	-1.000	0.999	86,517,647	86,517,785
16	87,864,576	87,982,384	2	-1.000	1.000	87,864,576	87,864,652
16	88,778,616	88,803,628	16	-0.964	0.964	88,798,124	88,798,185
17	1,069,486	1,132,504	24	-0.977	0.976	1,069,486	1,069,815
17	5,131,101	5,141,770	3	-1.000	1.000	5,131,101	5,134,242
17	5,653,386	5,656,808	2	-1.000	1.000	5,653,760	5,656,808
17	10,959,640	10,960,625	1	-0.998	0.998	10,959,640	10,960,625
17	11,705,627	12,013,909	56	-0.966	0.966	11,901,554	11,905,051
17	21,669,817	21,888,620	200	-0.983	0.977	21,851,196	21,859,777
17	24,061,686	24,080,243	6	-1.000	1.000	24,061,686	24,063,441
17	25,958,292	26,026,148	5	-0.977	0.977	25,980,835	25,982,718
17	53,542,771	53,872,457	324	-0.999	1.000	53,547,612	53,549,162
17	56,137,142	56,138,067	1	-1.000	1.000	56,137,142	56,138,067
17	65,298,000	65,311,245	3	-0.999	0.998	65,298,000	65,308,827
17	66,410,587	66,421,225	2	-0.998	0.998	66,410,587	66,411,932
17	67,719,145	67,722,916	4	-0.997	0.997	67,722,699	67,722,916
17	70,759,627	70,775,877	4	-0.981	0.981	70,759,627	70,767,324
17	79,826,290	79,887,923	29	-0.997	0.997	79,882,473	79,887,923
18	11,489,750	11,493,081	5	-1.000	1.000	11,489,750	11,490,819
18	25,156,004	25,175,957	26	-1.000	1.000	25,156,004	25,157,365
18	40,745,438	42,378,985	1347	-0.976	0.976	41,914,466	41,915,365
18	48,029,093	48,029,879	3	-0.987	0.988	48,029,736	48,029,879
18	51,492,618	51,501,041	3	-0.999	1.000	51,492,618	51,493,288
18	52,473,212	52,494,366	3	-1.000	1.000	52,489,432	52,494,366
18	55,140,378	55,436,867	403	-0.975	0.976	55,262,488	55,266,856
18	62,064,893	62,155,555	83	-0.958	0.982	62,154,982	62,155,555
19	2,681,193	3,137,975	200	-0.997	0.999	2,681,193	2,698,033
19	7,580,557	7,706,046	30	-0.995	0.994	7,612,904	7,613,057
19	20,270,797	20,303,241	19	-0.976	0.976	20,270,797	20,271,532
19	20,983,112	21,277,349	72	-0.973	0.972	20,996,946	20,997,874
19	38,524,709	38,526,386	2	-1.000	1.000	38,524,709	38,525,313
19	38,992,349	39,001,410	3	-0.999	0.999	38,994,650	39,001,410
19	45,745,329	45,748,959	1	-1.000	1.000	45,745,329	45,748,959
19	48,860,884	49,495,518	530	-0.967	0.965	48,860,884	48,862,177
19	56,321,034	56,332,147	5	-0.993	0.993	56,330,078	56,332,147
19	57,677,450	57,683,042	1	-1.000	1.000	57,677,450	57,683,042
19	60,519,669	60,528,783	3	-1.000	1.000	60,526,396	60,527,258
19	63,013,741	63,021,692	3	-1.000	1.000	63,013,741	63,015,210
20	4,482,749	4,499,234	3	-0.982	0.982	4,482,749	4,483,827
20	10,650,821	10,661,001	12	-1.000	1.000	10,659,826	10,661,001
20	11,931,267	11,996,018	78	-0.972	0.973	11,932,461	11,935,635
20	16,153,388	16,155,018	3	-1.000	1.000	16,153,388	16,154,403
20	18,293,048	18,375,219	37	-0.999	1.000	18,293,048	18,294,679
20	30,566,844	30,568,578	1	-1.000	1.000	30,566,844	30,568,578
20	41,116,748	41,127,580	3	-0.985	0.985	41,116,748	41,124,541
20	50,636,037	50,660,509	6	-0.992	0.992	50,659,279	50,660,509
20	53,565,192	53,579,405	8	-0.988	0.988	53,565,192	53,567,667
20	54,825,130	54,834,441	2	-0.998	0.999	54,825,130	54,832,167
20	56,280,471	56,288,277	4	-1.000	1.000	56,280,471	56,282,811
21	2,545,817	2,581,042	61	-0.966	0.968	2,545,817	2,546,686
21	9,989,585	10,006,121	8	-0.992	0.993	9,989,585	9,990,297
21	12,259,502	12,341,005	46	-0.958	0.958	12,259,502	12,259,637
21	17,040,828	17,177,593	162	-0.976	0.975	17,053,649	17,060,743
21	18,231,829	18,257,703	10	-0.976	0.976	18,254,349	18,257,703
21	21,630,893	21,638,700	9	-0.999	0.999	21,630,893	21,632,219
21	29,214,839	29,216,887	1	-1.000	1.000	29,214,839	29,216,887
21	30,545,515	30,552,622	2	-1.000	1.000	30,545,515	30,549,947
22	24,981,166	24,987,525	6	-0.997	0.997	24,981,166	24,981,439
22	31,809,221	31,817,286	3	-0.975	0.976	31,809,335	31,812,362
22	33,534,835	33,539,704	6	-0.996	0.995	33,534,835	33,536,131

22	34,825,691	34,827,264	1	-0.995	0.995	34,825,691	34,827,264
22	37,757,408	37,775,107	3	-0.998	0.998	37,757,408	37,760,872
22	41,001,347	41,012,097	4	-0.994	0.993	41,001,347	41,002,758
22	45,810,157	45,816,503	3	-0.997	0.997	45,810,157	45,810,593
22	47,481,333	47,488,195	2	-0.999	0.999	47,481,333	47,485,269
22	48,279,741	48,280,534	1	-1.000	1.000	48,279,741	48,280,534
22	49,572,377	49,575,651	1	-1.000	1.000	49,572,377	49,575,651

Table S3: The distribution of cross-over breakpoint resolutions. Breakpoint regions were defined as the sequence range containing the 95% credible interval spanning transmission vector switchpoints. Furthermore a ‘best guess’ range was calculated as the two consecutive sites with the largest change in the posterior probability. This table includes complex events that were resolved over > 1Mb.

	Break point length distribution (bases)				
Interval range percentile	2.50%	20%	50%	80%	97.50%
95% credible interval	754	2,555	8,752	49,328	1,260,462
Best guess SNV interval	54	331	1,230	3,149	10,633

Table S4: Cross-overs detected across five contigs on the pseudoautosomal region (PAR) each with length greater than 20 kb. The panTro3 PAR coordinates were defined as the interval syntenic with the location of PAR1 in GRCh37 (through liftOver). For children D - I, the number of female (F) and male-specific (M) crossovers are recorded. # POLY records the number of sites that pass filters and are polymorphic. # MENDEL INCONSISTENT records the number of sites that are not consistent with Mendel transmission. LLK TRANS. VEC. records the log-likelihood of the maximum likelihood transmission vector for that contig. PROP. CONSISTENT W. TRANS. VEC. represents the proportion of sites that are consistent with the maximum likelihood transmission vector.

	Contig start (bp)	Contig end (bp)	Number of cross-overs						# POLY.	# MENDEL INCONSISTENT	LLK TRANS. VEC.	PROP. CONSISTENT W. TRANS. VEC		
			D		E		F		G		H			
			F	M	F	M	F	M	F	M	F	M		
Contig 1	255,281	277,028									35	0	-3.30	0.94
Contig 2	676,430	700,287		1						1	57	3	-11.80	0.96
Contig 3	2,011,989	2,035,462								1	58	2	-2.13	1.00
Contig 4	2,330,840	2,391,726					1				172	3	-1.15	1.00
Contig 5	2,519,951	2,541,818					1				53	0	-1.51	0.90
Total cross-overs			0	0	0	1	0	0	1	1	0	0	0	2

Table S5: Sex-specific genetic distance across the pseudo-autosomal region in chimpanzees and humans. Chimpanzee values are calculated using Kosambi mapping function, human values are calculated as the weighted average of studies, which were each computed using the identity mapping function [38-40]. Rates are calculated using the total sequence for PAR1 in human GRCh37 and their liftover to panTro3 coordinates in chimpanzee. (^) : value from [17].

	Western chimpanzee		Human	
	Distance (cM)	Rate (cM/Mb)	Distance (cM)	Rate (cM/Mb)
PAR male-specific	34.657	16.085	49.528	18.764
PAR female-specific	8.664	3.217	4.06	1.538
Autosome sex-average		1.28		1.55^

Table S6: Listed are the de novo mutation candidates detected across the pedigree including false negatives. Locations are defined according to panTro3. Two quality metrics are presented: *pDepth* - the within-chunk combined depth percentile and *pAB* - the significance for deviation from the expected allele balance given the observed combined coverage. *Sequence context* represents the observed mutated allele flanked by 25 bases of surrounding sequence. *Allele0* and *Allele1* represent the reference and mutant alleles respectively. *Parental origin* indicates the inferred phase of the mutation (both direct read-based and transmission based phasing). *is_cpg* is an indicator variable marking mutations at CpGs. *is_suspicious* is an indicator variable recording our manual curation of the candidates.

Table S7: False positive rates estimated through re-genotyping at de novo mutation candidates in two non-founders E and F. Fractions represent the number of conflicting genotypes (assumed to be sequencing errors) over the total number of assayed sites; the rate is represented in brackets. *Trio consistency* denotes that the parental and the recipient child genotypes were consistent with the inferred mutation. *Pedigree consistency* denotes that the genotypes across the entire pedigree were consistent with the inferred genotypes.

Individual	Trio consistency	Pedigree consistency
E	1/36 (0.028)	1/35 (0.029)
F	0/25 (0)	0/24 (0)

Table S8: The estimated rate of false negatives in the point mutation detection approach, estimated through simulation on alignments (see Supplementary Text).

Individual	Transmission to F2	Number of missed simulated mutations	Total simulated	FNR
D		6	138	0.044
E		4	162	0.025
F		7	163	0.043
F ^a	{}	0	16	0.000
F ^b	{I}	1	16	0.063
F ^b	{H}	0	23	0.000
F ^b	{H,I}	1	20	0.050
F ^b	{G}	2	32	0.063
F ^b	{G,I}	0	18	0.000
F ^b	{I,H}	1	19	0.053
F ^b	{G,H,I}	2	19	0.105
G		35	153	0.229
H		36	152	0.237
I		34	152	0.224

^aAggregate values for F

^bValues for F marginalized over transmission to F2

Table S9: The total sequence of each individual's genome (unless otherwise specified) accessible to variation calling. The intersection mask was generated by taking the intersection of the sequence accessible to calling across the family. Sequence *accessible to variation calling* represents the total sequence passing filters on minimum coverage and mapping quality. The three remaining columns indicate the sequence failing each applied filter. Additionally, filters on homopolymer length, tandem repeat length, and insertion/deletion hotspots were applied to the panTro3 reference sequence and subtracted from the intersection mask; these are referred to as *reference filters*.

	Sequence accessible to variation calling (bp, % mappable genome)	Sequence failing filters						
		No coverage (bp, %mappable genome)	Coverage < 4 reads (bp, %mappable genome)	Proportion of reads with mapping quality < 1 exceeds 0.1 (bp, % mappable genome)				
A	2,625,654,085	95.354%	11,776,453	0.428%	11,461,457	0.416%	104,702,931	3.802%
B	2,611,551,977	94.842%	29,855,103	1.084%	15,555,201	0.565%	96,632,645	3.509%
C	2,622,647,354	95.244%	14,435,474	0.524%	31,864,036	1.157%	84,648,062	3.074%
D	2,623,685,945	95.282%	12,565,515	0.456%	20,481,221	0.744%	96,862,245	3.518%
E	2,623,912,927	95.290%	15,049,588	0.547%	36,213,785	1.315%	78,418,626	2.848%
F	2,614,415,878	94.946%	33,653,521	1.222%	20,698,310	0.752%	84,827,217	3.081%
G	2,621,362,476	95.198%	14,375,769	0.522%	34,117,425	1.239%	83,739,256	3.041%
H	2,621,596,116	95.206%	14,212,212	0.516%	33,167,882	1.205%	84,618,716	3.073%
I	2,619,595,151	95.134%	14,436,389	0.524%	29,333,844	1.065%	90,229,542	3.277%
Intersection	2,537,740,297	92.161%						
Intersection (Autosomes)	2,423,189,433							
Intersection (X)	114,284,786							
Intersection (Y)	266,078							
Reference filters applied (Autosomes)	2,360,347,379							
Reference filters applied (X)	111,402,572							

Bases assiged N 390,678,468
Bases not gaps or N, i.e. mappable genome 2,753,594,926

Table S10: Estimates of the number of point mutations in human and chimpanzees. The intercept and slope coefficients are estimated through Bayesian linear regression and are the posterior mean values.

	Western Chimpanzee	Human
Male intercept (mutations per generation) ^a	-23.80	-14.20
Female intercept (mutations per generation) ^a	6.65	14.20
Male slope (mutations per generation per paternal year) ^a	2.95	1.93
Female slope (mutations per generation per maternal year) ^a	0.00	0.00
Average paternal age (years) ^b	24.30	31.50
Average maternal age (years) ^b	26.30	25.60
Average mutations per generation (autosomes, haploid)	27.27	30.40
Average mutations per generation (X chromosome) ^c	20.40	25.00
Autosomal rate of divergence (mutations per year per genome)	1.08	1.06
X chromosome rate of divergence (mutations per year per genome equivalent)	0.80	0.91
Predicted X:A divergence	0.74	0.85
Autosomal diversity ^d (relative)	54.54	60.80
X chromosome diversity (relative)	30.59	37.50
Predicted X:A diversity	0.56	0.62
Proportion X chromosome mutations in female	0.22	0.38
Proportion A chromosome mutations in female	0.12	0.23
Alpha	7.20	3.28

^aHuman data from [16]

^bGeneration times from [20]

^cScaling male and female contributions by 1/3 and 2/3 respectively. Length of X scaled to be comparable to autosomes.

^dAssuming female and male effective population sizes are comparable.

Table S11: Analyses of point substitution divergence between human and chimpanzee. Spontaneous mutation estimates corrected for genomic regions where human and chimpanzee alignments are possible (see Supplement).

Divergence calculations for substitutions in the combined mask	
Autosomal substitutions (bases)	26,598,009
X chromosome substitutions (bases)	814,837
Autosomal sequence in combined mask (bases)	2,204,160,410
X Chromosome sequence in combined mask (bases)	86,111,635
Autosomal rate of divergence (substitution/base)	0.012
X chromosome rate of divergence (substitution/base)	0.010
X:A divergence	0.784
Estimated autosomal divergence time (using 2 x the chimpanzee mutation rate) (Million years)	13.475
Estimated autosomal divergence time (using chimpanzee and human mutation rates) (Million years)	11.247
Estimated X chromosome divergence time (using 2 x the chimpanzee mutation rate) (Million years)	14.179

Spontaneous mutation estimates for mutations in the combined mask	Chimpanzee	Human*
Male intercept (mutations per generation) ^a	-19.400	-14.200
Female intercept (mutations per generation) ^a	6.660	14.200
Male slope (mutations per generation per paternal year) ^a	2.600	1.930
Female slope (mutations per generation per maternal year) ^a	0.000	0.000
Average paternal age (years) ^b	24.300	31.500
Average maternal age (years) ^b	26.300	25.600
Average mutations per generation (autosomes, haploid)	34.326	34.014
Average mutations per year per genome (autosomes, haploid)	1.357	1.191
Average mutations per year per base	4.523E-10	3.971E-10
Average mutations per generation (X chromosome, haploid) ^c ; autosome equivalent	19.033	24.998
Average mutations per year (X chromosome, haploid); autosome equivalent	1.011	1.015
Average mutations per year per base (X chromosome) ^c	3.37E-10	3.38E-10

^aHuman data from [16]; all mutations are assumed to lie in the mask

^bGeneration times from [20]

^cScaling male and female contributions by 1/3 and 2/3 respectively. Length of X scaled to be comparable to autosomes.

^dAssuming female and male effective population sizes are comparable.

*Since only summary data was available, we were unable to apply the mask to the human mutation counts.

References and Notes

1. M. W. Nachman, S. L. Crowell, Estimate of the mutation rate per nucleotide in humans. *Genetics* **156**, 297–304 (2000). [Medline](#)
2. K. D. Makova, W. H. Li, Strong male-driven evolution of DNA sequences in humans and apes. *Nature* **416**, 624–626 (2002). [Medline](#) doi:10.1038/416624a
3. J. Taylor, S. Tyekucheva, M. Zody, F. Chiaramonte, K. D. Makova, Strong and weak male mutation bias at different sites in the primate genomes: Insights from the human-chimpanzee comparison. *Mol. Biol. Evol.* **23**, 565–573 (2006). [Medline](#) doi:10.1093/molbev/msj060
4. F. A. Kondrashov, A. S. Kondrashov, Measurements of spontaneous rates of mutations in the recent past and the near future. *Philos. Trans. R. Soc. Lond. B Biol. Sci.* **365**, 1169–1176 (2010). [Medline](#) doi:10.1098/rstb.2009.0286
5. J. C. Roach, G. Glusman, A. F. Smit, C. D. Huff, R. Hubley, P. T. Shannon, L. Rowen, K. P. Pant, N. Goodman, M. Bamshad, J. Shendure, R. Drmanac, L. B. Jorde, L. Hood, D. J. Galas, Analysis of genetic inheritance in a family quartet by whole-genome sequencing. *Science* **328**, 636–639 (2010). [Medline](#) doi:10.1126/science.1186802
6. D. F. Conrad, J. E. Keebler, M. A. DePristo, S. J. Lindsay, Y. Zhang, F. Casals, Y. Idaghdour, C. L. Hartl, C. Torroja, K. V. Garimella, M. Zilversmit, R. Cartwright, G. A. Rouleau, M. Daly, E. A. Stone, M. E. Hurles, P. Awadalla; 1000 Genomes Project, Variation in genome-wide mutation rates within and between human families. *Nat. Genet.* **43**, 712–714 (2011). [Medline](#) doi:10.1038/ng.862
7. A. Kong, M. L. Frigge, G. Masson, S. Besenbacher, P. Sulem, G. Magnusson, S. A. Gudjonsson, A. Sigurdsson, A. Jonasdottir, A. Jonasdottir, W. S. Wong, G. Sigurdsson, G. B. Walters, S. Steinberg, H. Helgason, G. Thorleifsson, D. F. Gudbjartsson, A. Helgason, O. T. Magnusson, U. Thorsteinsdottir, K. Stefansson, Rate of de novo mutations and the importance of father's age to disease risk. *Nature* **488**, 471–475 (2012). [Medline](#) doi:10.1038/nature11396
8. J. J. Michaelson, Y. Shi, M. Gujral, H. Zheng, D. Malhotra, X. Jin, M. Jian, G. Liu, D. Greer, A. Bhandari, W. Wu, R. Corominas, A. Peoples, A. Koren, A. Gore, S. Kang, G. N. Lin, J. Estabillo, T. Gadomski, B. Singh, K. Zhang, N. Akshoomoff, C. Corsello, S. McCarroll, L. M. Iakoucheva, Y. Li, J. Wang, J. Sebat, Whole-genome sequencing in autism identifies hot spots for de novo germline mutation. *Cell* **151**, 1431–1442 (2012). [Medline](#) doi:10.1016/j.cell.2012.11.019
9. A. Scally, R. Durbin, Revising the human mutation rate: Implications for understanding human evolution. *Nat. Rev. Genet.* **13**, 745–753 (2012). [Medline](#) doi:10.1038/nrg3295
10. J. F. Crow, The origins, patterns and implications of human spontaneous mutation. *Nat. Rev. Genet.* **1**, 40–47 (2000). [Medline](#) doi:10.1038/35049558
11. T. Miyata, H. Hayashida, K. Kuma, K. Mitsuyasu, T. Yasunaga, Male-driven molecular evolution: A model and nucleotide sequence analysis. *Cold Spring Harb. Symp. Quant. Biol.* **52**, 863–867 (1987). [Medline](#) doi:10.1101/SQB.1987.052.01.094
12. D. C. Presgraves, S. V. Yi, Doubts about complex speciation between humans and chimpanzees. *Trends Ecol. Evol.* **24**, 533–540 (2009). [Medline](#) doi:10.1016/j.tree.2009.04.007
13. Supplementary materials are available on *Science* Online.

14. Z. Iqbal, M. Caccamo, I. Turner, P. Flicek, G. McVean, De novo assembly and genotyping of variants using colored de Bruijn graphs. *Nat. Genet.* **44**, 226–232 (2012). [Medline](#) [doi:10.1038/ng.1028](#)
15. J. W. IJdo, A. Baldini, D. C. Ward, S. T. Reeders, R. A. Wells, Origin of human chromosome 2: An ancestral telomere-telomere fusion. *Proc. Natl. Acad. Sci. U.S.A.* **88**, 9051–9055 (1991). [Medline](#) [doi:10.1073/pnas.88.20.9051](#)
16. A. Kong, G. Thorleifsson, D. F. Gudbjartsson, G. Masson, A. Sigurdsson, A. Jonasdottir, G. B. Walters, A. Jonasdottir, A. Gylfason, K. T. Kristinsson, S. A. Gudjonsson, M. L. Frigge, A. Helgason, U. Thorsteinsdottir, K. Stefansson, Fine-scale recombination rate differences between sexes, populations and individuals. *Nature* **467**, 1099–1103 (2010). [Medline](#) [doi:10.1038/nature09525](#)
17. A. Kong, D. F. Gudbjartsson, J. Sainz, G. M. Jonsdottir, S. A. Gudjonsson, B. Richardsson, S. Sigurdardottir, J. Barnard, B. Hallbeck, G. Masson, A. Shlien, S. T. Palsson, M. L. Frigge, T. E. Thorgeirsson, J. R. Gulcher, K. Stefansson, A high-resolution recombination map of the human genome. *Nat. Genet.* **31**, 241–247 (2002). [Medline](#)
18. A. Auton, A. Fledel-Alon, S. Pfeifer, O. Venn, L. Ségurel, T. Street, E. M. Leffler, R. Bowden, I. Aneas, J. Broxholme, P. Humburg, Z. Iqbal, G. Lunter, J. Maller, R. D. Hernandez, C. Melton, A. Venkat, M. A. Nobrega, R. Bontrop, S. Myers, P. Donnelly, M. Przeworski, G. McVean, A fine-scale chimpanzee genetic map from population sequencing. *Science* **336**, 193–198 (2012). [Medline](#) [doi:10.1126/science.1216872](#)
19. J. Marson, S. Meuris, R. W. Cooper, P. Jouannet, Puberty in the male chimpanzee: Progressive maturation of semen characteristics. *Biol. Reprod.* **44**, 448–455 (1991). [Medline](#) [doi:10.1095/biolreprod44.3.448](#)
20. K. E. Langergraber, K. Prüfer, C. Rowley, C. Boesch, C. Crockford, K. Fawcett, E. Inoue, M. Inoue-Muruyama, J. C. Mitani, M. N. Muller, M. M. Robbins, G. Schubert, T. S. Stoinski, B. Viola, D. Watts, R. M. Wittig, R. W. Wrangham, K. Zuberbühler, S. Pääbo, L. Vigilant, Generation times in wild chimpanzees and gorillas suggest earlier divergence times in great ape and human evolution. *Proc. Natl. Acad. Sci. U.S.A.* **109**, 15716–15721 (2012). [Medline](#) [doi:10.1073/pnas.1211740109](#)
21. G. H. Perry, J. C. Marioni, P. Melsted, Y. Gilad, Genomic-scale capture and sequencing of endogenous DNA from feces. *Mol. Ecol.* **19**, 5332–5344 (2010). [Medline](#) [doi:10.1111/j.1365-294X.2010.04888.x](#)
22. C. Hvilsom, Y. Qian, T. Bataillon, Y. Li, T. Mailund, B. Sallé, F. Carlsen, R. Li, H. Zheng, T. Jiang, H. Jiang, X. Jin, K. Munch, A. Hobolth, H. R. Siegismund, J. Wang, M. H. Schierup, Extensive X-linked adaptive evolution in central chimpanzees. *Proc. Natl. Acad. Sci. U.S.A.* **109**, 2054–2059 (2012). [Medline](#) [doi:10.1073/pnas.1106877109](#)
23. N. Patterson, D. J. Richter, S. Gnerre, E. S. Lander, D. Reich, Genetic evidence for complex speciation of humans and chimpanzees. *Nature* **441**, 1103–1108 (2006). [Medline](#) [doi:10.1038/nature04789](#)
24. R. V. Short, Sexual selection and its component parts, somatic and genital selection, as illustrated by man and the great apes. *Adv. Stud. Behav.* **9**, 131–158 (1979).

25. A. P. Møller, Ejaculate quality, testes size and sperm competition in primates. *J. Hum. Evol.* **17**, 479–488 (1988). [doi:10.1016/0047-2484\(88\)90037-1](https://doi.org/10.1016/0047-2484(88)90037-1)
26. The Chimpanzee Sequencing and Analysis Consortium, Initial sequence of the chimpanzee genome and comparison with the human genome. *Nature* **437**, 69–87 (2005). [Medline doi:10.1038/nature04072](https://doi.org/10.1038/nature04072)
27. G. Lunter, M. Goodson, Stampy: A statistical algorithm for sensitive and fast mapping of Illumina sequence reads. *Genome Res.* **21**, 936–939 (2011). [Medline doi:10.1101/gr.111120.110](https://doi.org/10.1101/gr.111120.110)
28. <http://www.well.ox.ac.uk/platypus>.
29. L. J. Peacock, C. M. Rogers, Gestation period and twinning in chimpanzees. *Science* **129**, 959 (1959). [Medline doi:10.1126/science.129.3354.959](https://doi.org/10.1126/science.129.3354.959)
30. S. B. Montgomery, D. L. Goode, E. Kvikstad, C. A. Albers, Z. D. Zhang, X. J. Mu, G. Ananda, B. Howie, K. J. Karczewski, K. S. Smith, V. Anaya, R. Richardson, J. Davis, D. G. MacArthur, A. Sidow, L. Duret, M. Gerstein, K. D. Makova, J. Marchini, G. McVean, G. Lunter; 1000 Genomes Project Consortium, The origin, evolution, and functional impact of short insertion-deletion variants identified in 179 human genomes. *Genome Res.* **23**, 749–761 (2013). [Medline doi:10.1101/gr.148718.112](https://doi.org/10.1101/gr.148718.112)
31. Z. Iqbal, I. Turner, G. McVean, High-throughput microbial population genomics using the Cortex variation assembler. *Bioinformatics* **29**, 275–276 (2013). [Medline doi:10.1093/bioinformatics/bts673](https://doi.org/10.1093/bioinformatics/bts673)
32. E. S. Lander, P. Green, Construction of multilocus genetic linkage maps in humans. *Proc. Natl. Acad. Sci. U.S.A.* **84**, 2363–2367 (1987). [Medline doi:10.1073/pnas.84.8.2363](https://doi.org/10.1073/pnas.84.8.2363)
33. G. R. Abecasis, S. S. Cherny, W. O. Cookson, L. R. Cardon, Merlin—rapid analysis of dense genetic maps using sparse gene flow trees. *Nat. Genet.* **30**, 97–101 (2002). [Medline doi:10.1038/ng786](https://doi.org/10.1038/ng786)
34. A. G. Hinch, A. Tandon, N. Patterson, Y. Song, N. Rohland, C. D. Palmer, G. K. Chen, K. Wang, S. G. Buxbaum, E. L. Akylbekova, M. C. Aldrich, C. B. Ambrosone, C. Amos, E. V. Bandera, S. I. Berndt, L. Bernstein, W. J. Blot, C. H. Bock, E. Boerwinkle, Q. Cai, N. Caporaso, G. Casey, L. Adrienne Cupples, S. L. Deming, W. Ryan Diver, J. Divers, M. Fornage, E. M. Gillanders, J. Glessner, C. C. Harris, J. J. Hu, S. A. Ingles, W. Isaacs, E. M. John, W. H. Linda Kao, B. Keating, R. A. Kittles, L. N. Kolonel, E. Larkin, L. Le Marchand, L. H. McNeill, R. C. Millikan, Murphy, S. Musani, C. Neslund-Dudas, S. Nyante, G. J. Papanicolaou, M. F. Press, B. M. Psaty, A. P. Reiner, S. S. Rich, J. L. Rodriguez-Gil, J. I. Rotter, B. A. Rybicki, A. G. Schwartz, L. B. Signorello, M. Spitz, S. S. Strom, M. J. Thun, M. A. Tucker, Z. Wang, J. K. Wiencke, J. S. Witte, M. Wrensch, X. Wu, Y. Yamamura, K. A. Zanetti, W. Zheng, R. G. Ziegler, X. Zhu, S. Redline, J. N. Hirschhorn, B. E. Henderson, H. A. Taylor Jr., A. L. Price, H. Hakonarson, S. J. Chanock, C. A. Haiman, J. G. Wilson, D. Reich, S. R. Myers, The landscape of recombination in African Americans. *Nature* **476**, 170–175 (2011). [Medline doi:10.1038/nature10336](https://doi.org/10.1038/nature10336)
35. D. Kosambi, The estimation of map distances from recombination values. *Ann. Eugen.* **12**, 172–175 (1944).
36. D. Karolchik, G. P. Barber, J. Casper, H. Clawson, M. S. Cline, M. Diekhans, T. R. Dreszer, P. A. Fujita, L. Guruvadoo, M. Haeussler, R. A. Harte, S. Heitner, A. S. Hinrichs, K. Learned, B. T. Lee, C. H. Li, B. J. Raney, B. Rhead, K. R. Rosenbloom,

- C. A. Sloan, M. L. Speir, A. S. Zweig, D. Haussler, R. M. Kuhn, W. J. Kent, The UCSC Genome Browser database: 2014 update. *Nucleic Acids Res.* **42**, D764–D770 (2014). [Medline](#)
37. A. McKenna, M. Hanna, E. Banks, A. Sivachenko, K. Cibulskis, A. Kernytsky, K. Garimella, D. Altshuler, S. Gabriel, M. Daly, M. A. DePristo, The Genome Analysis Toolkit: A MapReduce framework for analyzing next-generation DNA sequencing data. *Genome Res.* **20**, 1297–1303 (2010). [Medline doi:10.1101/gr.107524.110](#)
38. A. Henke, C. Fischer, G. A. Rappold, Genetic map of the human pseudoautosomal region reveals a high rate of recombination in female meiosis at the Xp telomere. *Genomics* **18**, 478–485 (1993). [Medline doi:10.1016/S0888-7543\(11\)80003-0](#)
39. D. C. Page, K. Bieker, L. G. Brown, S. Hinton, M. Leppert, J. M. Lalouel, M. Lathrop, M. Nystrom-Lahti, A. de la Chapelle, R. White, Linkage, physical mapping, and DNA sequence analysis of pseudoautosomal loci on the human X and Y chromosomes. *Genomics* **1**, 243–256 (1987). [Medline doi:10.1016/0888-7543\(87\)90051-6](#)
40. F. Rouyer, M. C. Simmler, C. Johnsson, G. Vergnaud, H. J. Cooke, J. Weissenbach, A gradient of sex linkage in the pseudoautosomal region of the human sex chromosomes. *Nature* **319**, 291–295 (1986). [Medline doi:10.1038/319291a0](#)